Shrinkage behavior enhancement of infra-lightweight concrete through FRP grid reinforcement and development of their shrinkage prediction models

Yue Liu[a], T. Tafsirojjaman[b,*], Attiq Ur Rahman Dogar[c], Alexander Hückler[d]

[a] The Key Laboratory of Urban Security and Disaster Engineering of Ministry of Education, Beijing University of Technology, 100 Pingleyuan, Beijing, China

[b] School of Civil and Environmental Engineering, Faculty of Science and Engineering, Queensland University of Technology, 2 George Street, Brisbane, QLD 4000, Australia.

[c] Department of Civil Engineering, University of Central Punjab, Lahore, Pakistan.

[d] Chair of Conceptual and Structural Design, Institute of Civil Engineering, Technische Universität Berlin, Berlin, Germany

(*Corresponding author: tafsirojjaman@hdr.qut.edu.au (T. Tafsirojjaman)

Abstract:

Infra-lightweight concrete (ILC) is an efficient alternative of normal concrete (NC) for structural applications with low strength but high thermal performance requirements. Three types of ILCs with dry densities 600, 700 and 800 kg/m^3 have been manufactured by using high water to cement ratio (*w*/*c*) and expanded clay lightweight aggregates (ECLAs). Experimental studies showed that shrinkage strains in ILCs are greater than 1.2 mm/m as compared to 0.2-0.8 mm/m for NCs, which affects the structural durability of ILCs. To control shrinkage strains of ILCs, ILCs have been then reinforced with two types of fiber reinforced polymers (FRPs): carbon fiber reinforced polymer (CFRP) and glass fiber reinforced polymer (GFRP). For each type of FRP, two different grid

arrangements of size 21×21 mm and 25×25 mm have been used. Although all FRP grid reinforcements are effective as they reduced the shrinkage strains significantly and close to the shrinkage strains of NCs, CFRP reinforcement with 25×25 mm grid is most effective as it reduced the shrinkage strains up-to the maximum level. Also, experimental shrinkage strains have been compared with five commonly used prediction models and it has been found that each model failed to accurately predict the shrinkage strains. Therefore, a new prediction model has been developed by modifying one of the existing model i.e. B3 model for shrinkage prediction of ILC which considers the effect of water content, compressive strength and dry density. Another prediction model for FRP reinforced ILCs has also been developed to incorporate the influence of any type of reinforcement in ILC. A comparison of modified prediction models with experimental results has shown that the models can predict shrinkage accurately and can be utilized for normal ILC as well as reinforced ILCs.

Keywords: Infra-lightweight concrete (ILC); shrinkage strains; FRP reinforced ILC; shrinkage prediction model of ILC; shrinkage prediction model of reinforced ILC.

1. Introduction:

The exploitation of natural resources and the production of a large amount of construction waste have alarmed serious concerns about economic and environmental sustainability. Meyer [1] reported that concrete alone is responsible for the consumption of 1.2 billion tons of cement and 7.5 billion tons of aggregates annually. Also, most of the construction waste is not recyclable which poses serious environmental threats. Increasing awareness about sustainable development has urged the researchers and concrete producers to use environmentally friendly and recycled materials for concrete production to reduce environmental and economic impacts [2].

Effective utilization of natural resources also involves altering the properties of concrete considering both strength and energy efficiency requirements. Normal concrete (NC) has a high unit weight ranging between 2200 to 2600 kg/m^3 as well as the high thermal conductivity of 1.4 to 3.6 W/m·C [3] which makes it unsuitable for application where strength requirements are low but energy efficiency requirements are high e.g. walls. For such applications, lightweight concrete is a suitable alternative having a unit weight ranging from 800 to 2000 kg/m^3 and thermal conductivity as high as 1 W/m·C [4]. Lightweight concrete (LC) is normally manufactured by using lightweight aggregates which can either be natural e.g. diatomite, pumice etc. or artificial i.e. expanded or plastic aggregates. A significant amount of research studies on LC have been carried out related to various mix design procedures, workability and compressive strength, durability and shrinkage [5-8]. In spite of its various advantages over NC, LC has disadvantages regarding its durability. As a higher water-cement (*w*/*c*) ratio is used for its manufacture, drying shrinkage also increases due to self-desiccation and water loss during its drying process. This shrinkage of concrete in constrained condition produces tensile stresses and leads to initiation and propagation of cracking [7], corrosion of reinforcement, and ultimately reduces the service life of concrete structures. According to Neville [8], initial drying shrinkage of LCs can be 5 to 40 % higher than the normal weight and total shrinkage can be even higher. Reinhardt and Kummel [9] conducted a study on LC by replacing natural aggregate with expanded lightweight clay aggregates and concluded that shrinkage increment was around 50 % for concrete with 54 % replaced aggregates. In another study by Hansen and Boegh [10], 70 % shrinkage was measured when natural aggregates were completely replaced by recycled concrete aggregates. As the wide variety of materials are used to produce LC, the shrinkage strains in each type differ and Kayali et al. [11]

recommended to consider properties of aggregates to ascertain their effect on shrinkage of concrete.

In addition to studying the shrinkage behavior of LC, significant amount of research studies have also been conducted to reduce this shrinkage. This shrinkage in LC can be reduced by using either shrinkage reducing admixtures (SRAs), fiber reinforcement or through internal curing (IC). The addition of SRAs reduces the surface tension of water in concrete resulting in a lower rate of evaporation, modification of morphology of hydrated cement paste and lower shrinkage and creep strains. Experimental studies conducted by Shh et al. [12], Shoya et al. [13] and Berke et al. [14] showed that SRAs can reduce the concrete shrinkage by up-to 50 %, improve restrained shrinkage performance, increase the time for the appearance of the first crack and reduces crack widths as well. However, the addition of SRAs can affect the mechanical properties of concrete and Shh et al. [12] showed that the addition of SRAs can reduce the compressive strength of concrete by 10-25 %. A suitable alternative for reducing the effect of concrete shrinkage on structural performance without compromising the strength properties of concrete is fiber reinforcement i.e. glass, steel, carbon or polymer. Fiber reinforcement polymers (FRP) have the higher tensile strength [15], very low weight-strength ratio [16], highly corrosion resistive [17] and better flexibility [18] etc. The addition of fiber reinforcement reduces the shrinkage cracking in the early days and permeability of concrete in service conditions [19]. It has also been reported that the addition of FRPs can increase the tensile strength by 100%, compressive strength by 10–25 % and flexural strength by 150–200% [20]. Initial shrinkage can also be controlled through internal curing using pre-wetted lightweight aggregates (PWLAs) which provide moisture to compensate for the loss of water during hydration. Wang et al. [21] reported the shrinkage studies conducted using PWLAs and also showed that increasing the amount of PWLAs also reduces the strength gain in concrete. Out

of all the alternatives, the addition of FRPs can be more effective as it reduces the shrinkage strains and can also increase the strength of concrete.

As the shrinkage strains in LC depend on the type of aggregates and mix proportion of concrete, prediction of early age and long-term concrete shrinkage is crucial during analysis and design to investigate its impact on structural durability and performance. As there are different types of aggregates used for the production of LC and controlling this shrinkage, types of shrinkage models and their usage also differs. From a range of available models, five commonly used shrinkage prediction models are ACI 209R-92 model [22], CEB MC90-99 model [23], Eurocode-2 model [24], B3 model [25] and AS 3600 model [26]. A systematic review of all these prediction models using recycled aggregates has been reported by Silva et al. [27] who compared the experimental results of a number of concrete mixes with prediction models. All these prediction models have been developed based on a range of experimental data and can only give accurate results based on specific satisfied conditions in which tests were carried out. A number of conditions affecting the shrinkage should be considered to predict them including concrete mix proportions, the compressive strength of concrete, age of concrete, method of curing, type of cement, type of aggregates, *w*/*c* ratio, shape and size of member etc. As the types of LCs differ according to aggregates used and manufacturing conditions, parameters used in the prediction models must be studied precisely to ascertain the accuracy of these models.

Recently, Infra-lightweight concrete (ILC) was manufactured at Technische Universität Berlin (TU Berlin) to be used as exterior walls of concrete structures [28]. The term infra in ILC means below and thus ILC can be defined as a high-performance concrete (HPC) with unit weight equal to or less than 800 kg/m^3 [29]. Low dry density, adequate strength to weight ratio, low thermal conductivity and freeform surface makes it a superior alternative of masonry and NC walls [30].

Design and construction specifications for ILC have also been developed and well documented [31]. Single story houses have been built in Germany with exterior walls made of ILC and they have demonstrated its practicality and potential for excellent thermal and mechanical properties [32]. However, shrinkage strains in these houses are significantly higher as compared to NC as well as the values obtained through shrinkage prediction models. As the prediction models have been developed only for NC under specific conditions, development of prediction models for ILCs is critical for its accurate shrinkage determination. Also, higher shrinkage strains in ILCs should also be controlled to avoid excessive cracking and reinforcement corrosion to improve structural durability. However, there is no literature available for shrinkage determination of ILC and control of this shrinkage. Therefore, in this research program, detailed experimental tests have been conducted to evaluate the mechanical and thermal properties and shrinkage strains of ILCs. Three types of ILCs have been manufactured with dry densities of 600, 700 and 800 kg/m^3 and termed as ILC600, ILC700 and ILC800 respectively. To control the shrinkage, these ILCs have been then reinforced with two types of FRPs: carbon fiber reinforced polymer (CFRP) and glass fiber reinforced polymer (GFRP), and two different grid arrangements (21 mm and 25 mm) for each type of FRP i.e. CFRP-21, CFRP-25, GFRP-21 and GFRP-25 have been used. Since ILCs have been developed as a thermally insulated lightweight wall, traditional use of steel as shrinkage reinforcement is not a feasible option. Firstly, thermal conductivity of steel is significantly higher than FRPs and its presence in ILC creates a thermal bridge and hinders its insulation efficiency [33]. Secondly, higher unit weight of steel as compared to CFRP and GFRP bars will result in higher weight of reinforced ILC [34]. Also, higher shrinkage strains and porosity in ILC makes the reinforcement susceptible to corrosion due to which use of steel reinforcement will cause durability problems and the rusting and expanding of the steel reinforcement will also make the

ILC crack and spall [34]. Considering these practical aspects, CFRP and GFRP bars have been preferred over conventional steel reinforcement.

Experimental studies have also shown that shrinkage strains in ILCs are higher than that of NC and FRPs can significantly reduce the shrinkage strains. Although all the FRP grid reinforcements are effective as they reduced the shrinkage strains significantly, closer to the shrinkage strains of NC, CFRP-25 grid reinforcement is most effective as it reduced the shrinkage strains up-to the maximum level. Shrinkage strains of ILCs have been calculated analytically using five commonly used prediction models i.e. the ACI 209R-92 [22], the CEB MC90-99 model [23], the Eurocode-2 model [24], B3 model [25] and AS 3600 model [26]. The comparison of experimentally obtained shrinkage strains with that of predicted strains for all the ILCs have revealed that none of these models can predict the shrinkage strains in ILC accurately. Therefore, two new prediction models based on the B3 model have been developed in this research study, one for normal ILCs and one for reinforced ILCs. The comparison of experimental results with newly developed prediction models has shown that both developed prediction models accurately predict the shrinkage strains of normal ILCs and FRP reinforced ILCs and these models can be adopted for shrinkage calculation of normal ILCs and ILCs with any type of reinforcement.

2. Experimental Programs

2.1 Materials

Three types of ILCs have been prepared with varying dry densities i.e. 600, 700 and 800 kg/m^3. These ILCs have been termed as ILC600, ILC700 and ILC800 respectively based on their dry densities. The lightweight of concrete is achieved by replacing normal aggregates by expanded lightweight clay aggregates (ELCAs). Two types of ELCAs were used i.e. 1/4 (grain size from 1 mm to 4 mm) and 2/6 (grain size from 2 mm to 6 mm). The reason for using ECLA was that it

requires low air-entrainment as compared to autoclaved concrete where LC is obtained by high air content. This low air entrainment results in higher compressive strength of concrete as compared to autoclave concrete. In addition of ECLAs, lightweight sand with particle size ranging from 0 to 1 mm has been used as fine aggregates. Pphysical and chemical properties of ELCAs and sand are given in Table 1.

Blast furnace slag cement with grade CEM III/A 32.5 N has been used. CEM III is a mixture of OPC and blast furnace slag and has three types: A, B and C. A contains the least slag of 40%. 32.5 is the strength grade of cement and N refers to the class of cement with ordinary early strength. According to the ASTM C150 [35], the CEM III/A 32.5 N is classified as Type II cement with moderate heat of hydration and moderate sulfate resistance. Two types of admixtures have been used in ILC i.e. plasticizer and stabilizer. The plasticizer reduces the water demand in fresh concrete, which can either reduce the water content or improve the processability (flowability) while maintaining the same *w*/*c* value. The stabilizer prevents fresh concrete from segregating especially in the case of LC. No admixture has been used for air-entrainment as the lightweight of ILC is obtained by using ECLAs.

Table 1: Physical and chemical properties of ECLAs and sand

Essential characteristics		1/4 ECLA	2/6 ECLA	Lightweight sand
Physical Properties	Particle shape	Round	Round	Crushed
	Particle size (mm)	1-4 mm	2-6 mm	0-1 mm
	Fines	≤ 3.0 M.-%	≤ 1.5 M.-%	-
	Loose bulk density ($kg/m^{3)}$	450 ± 65	290 ± 25	700±50
	Particle density (kg/m^3)	0.85 ± 0.125	0.54 ± 0.05	1.78 ± 0.1
	Water absorption, w_{60}(%)	9± 4 M.-%	11± 4 M.-%	-
	Water absorption, w_{24h}(%)	11 ± 4 M.-%	14 ± 4 M.-%	-
	Crushing resistance (N/mm^2)	≥ 3	≥ 0.9	-
	Water content	-	-	≤ 1.0 M.-%
Chemical Properties	Chloride	≤ 0.02 M.-%	≤ 0.02 M.-%	≤ 0.02 M.-%
	Acid-soluble sulfate	≤ 0.8 M.-%	≤ 0.8 M.-%	≤ 0.8 M.-%
	Total sulfur	≤ 1.0 M.-%	≤ 1.0 M.-%	≤ 1.0 M.-%

2.2 Sample preparation:

For each type of ILC, three samples have been prepared to make a total of 9 samples. Mix proportions of materials to prepare each type of ILC are given in Table 2. From Table 2, it can be seen that the amount of sand required for each ILC increases with the increases in dry density. As the lightweight of concrete is achieved by expanded clay lightweight aggregates (ECLAs) instead of air-entrainment, the mass of total lightweight aggregates (1/4 and 1/6) decreases with increase in ILC's dry density. This sum is maximum for ILC600 i.e. 314 kg/m^3 and minimum for ILC800

i.e. 261 kg/m^3 of concrete. Although the amount of cement and water content increases with the increase in ILC's density, the corresponding *w*/*c* ratios decrease which is 1.13 for ILC600, 0.90 for ILC700 and 0.77 for ILC800. This higher *w*/*c* ratio aids in decreasing the dry density of ILC. The amount of silica fumes and the volume of entrained air are almost constant for each type of ILC. As the *w*/*c* ratio decreases with an increase in ILC's density, the amount of plasticizer and stabilizer increases to improve the workability. To compare the proportions, the mix design composition of a normal weight concrete (NC 30/37) having a density of 2306 kg/m^3 is also given in Table 2.

In addition to normal ILCs, ILCs with carbon and glass fiber reinforcements (CFRPs and GFRPs) have also been prepared to examine their effect on shrinkage strains. For each type of FRP, two different grid arrangements have been used and named as CFRP-21, CFRP-25, GFRP-21 and GFRP-25. The numbers 21 and 25 indicate the width and height of the FRP grid respectively (Figure 1) and their descriptions and properties are given in Table 3. From properties in Table 3, it is evident that strength, as well as elastic modulus of CFRPs, is twice than that of GFRPs for the same cross-sectional area. Also, the cross-sectional area per unit length of 25 mm FRP grid is greater than that of 21 mm FRP grid. The grid dimensions are presented in Figure 1 b & c. For example, the total cross-sectional area of longitudinal reinforcement for CFRP-21 can be calculated as 85 mm^2/m × 21 mm × 4/1000 mm/m = 7.14 mm^2 giving a reinforcement ratio of 7.14 mm^2 / (40 mm × 40 mm) × 100% = 0.45 %. Eurocode 2 [24] for design of concrete structures recommends a reinforcement ratio in range of 0.2% to 4% for reinforced concrete walls. Similarly, ACI 318 [36] suggests a minimum reinforcement ratio of 0.15% for reinforced concrete walls. As the reinforcement ratios in ILCs are between 0.45% and 0.91%, therefore, reinforcements

requirements of both the codes have been met. For each type ILC with a single grid arrangement of FRP, 3 samples were prepared to make a total of 3 × 4 × 3 = 36 FRP reinforced samples.

Table 2: Mix Proportions for ILCs [28] and NC

Material	ILC 600		ILC 700		ILC 800			NC (30/37)	
	V (L)	M (kg)	V (L)	M (kg)	V (L)	M (kg)		V (L)	M (kg)
Sand	7	19	17	47	26	72	Sand	340	883
Aggregate1/4	118	118	108	108	98	98	Gravel 2/6	322	837
Aggregate 2/6	325	198	283	173	240	147			
CEM III-A	62	188	85	260	109	333	CEM III-A	128	391
Water	214	214	234	234	255	255	Water	195	195
Silica fume	31	73	30	71	28	66			
Plasticizer	2.65	2.86	2.95	3.19	3.26	3.52			
Stabilizer	0.3	0.27	0.5	0.45	0.7	0.63			
Air	240	0	240	0	240	0	Air	15	0
Sum	1000	813	1000	897	1000	975	Sum	1000	2306

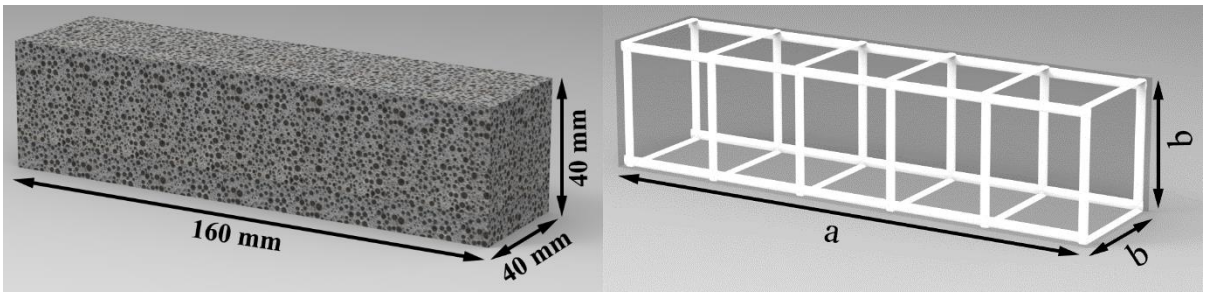

(a)

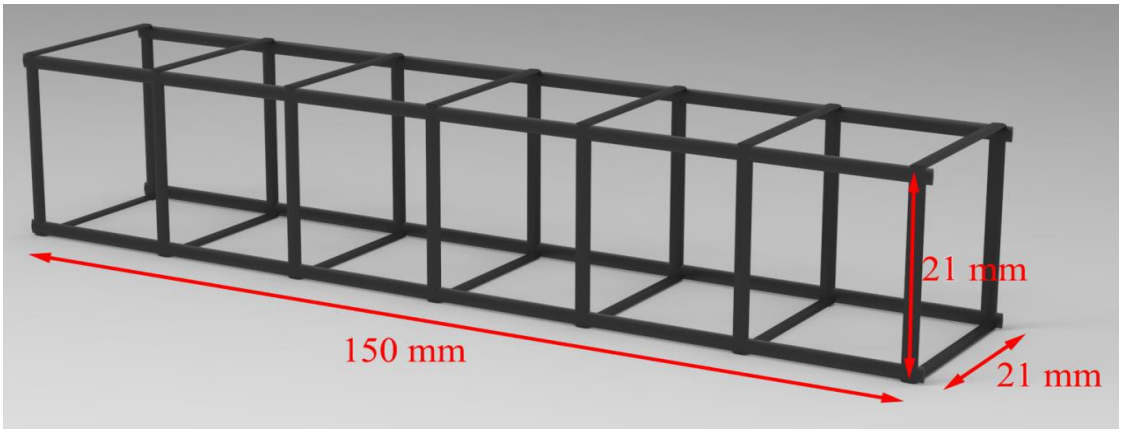

(b)

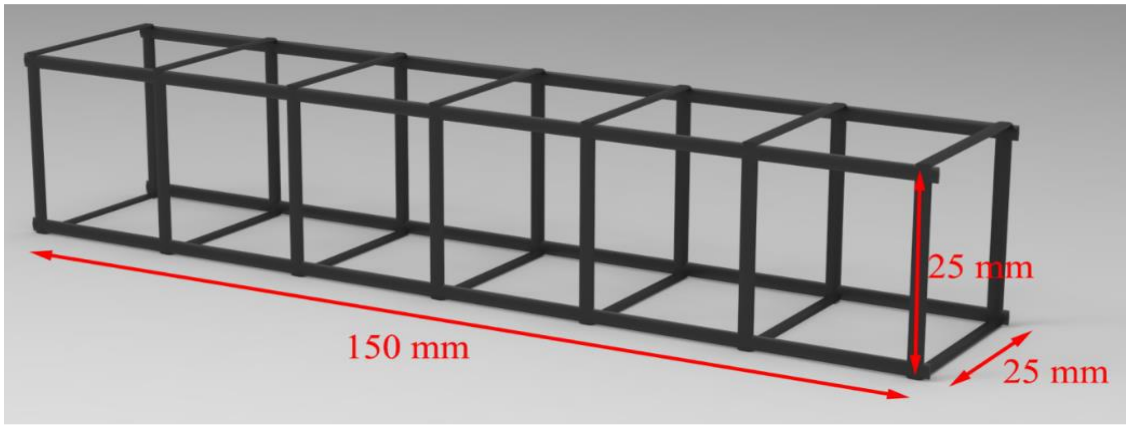

(c)

Figure 1: Specimen Details (a) prism and FRP grid dimensions (b) FRP-21 (c) FRP-25

Table 3: FRP grid dimensions and properties

FRP	Width of one grid (mm)	Cross sectional area per unit length* (mm^2/m)	FRP reinforcement ratio (%)	Strength (MPa)	Elastic Modulus (GPa)	a (mm)	b (mm)
CFRP-21	21	85	0.45	2300	120	150	21
CFRP-25	25	142	0.89	2300	120	150	25
GFRP-21	21	87	0.46	1100	60	150	21
GFRP-25	25	145	0.91	1100	60	150	25

* Cross-sectional area of reinforcement per unit length in the both directions of the grid

2.3 Testing

The specimens prepared from mentioned mixes have been tested for mechanical and thermal properties and dry shrinkage strains as per European standards. Mechanical and thermal properties include dry density, cylinder compressive strength, tensile strength and modulus of elasticity. Dry densities of oven-dried samples at the temperature range of 105±5^{o}C as recommended by BS-EN-12390-7 [37] have been measured. Cylinder compressive strength (f_c) tests have been carried out on 150x300 mm cylinders cylinders at the age of 28 days as recommended by BS-EN-206 [38]. For tensile strength, three-point bending tests on 40×40×160 mm prisms have been carried out as per BS-EN-196-1 [39] and elastic moduli of 150×300 mm cylinders have been measured at the age of 28 days according to BS-EN-12390-13 [40].

Dry shrinkage tests have been conducted according to BS-EN-12617-2002 [41] (Figure 2). According to this standard, drying shrinkage strains in concrete should be determined by measuring unrestrained linear movement of prismatic specimens 160×40×40 mm in size.

Therefore, specimens of similar size have been prepared for both the normal and reinforced ILCs. For each ILC grade, three specimens have been prepared and kept in climatic conditions of 20^{o}C and 65% humidity. Shrinkage strains have been measured with micrometer length compactor for 2, 3, 7, 14, 28, 50, 100 days of concrete age.

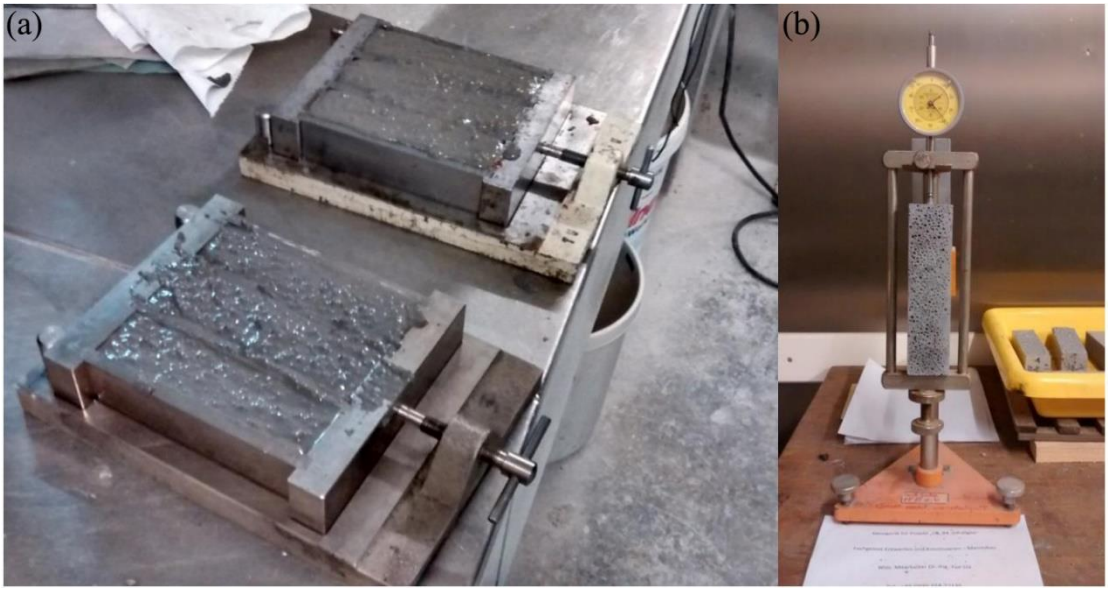

Figure 2: Shrinkage test (a) specimen casting and (b) shrinkage measuring

3. Experimental results and discussions:

3.1 Mechanical and thermal properties of ILCs:

Mechanical and thermal properties including dry density, compressive strength, tensile strength, modulus of elasticity and thermal conductivity coefficient are given in Table 4. BS-EN-206 defines lightweight concrete as the concrete with dry density in the range of 800 to 2000 kg/m^3. As the dry density of tested concrete is equal to and less than 800 kg/m^3, therefore, it has been termed as infra-lightweight concrete (ILC). Also, minimum characteristic cylinder strength as per BS-EN-206 [38] for LC8/9 is 8 N/mm^2 respectively. However, the tested cylinder strength for ILC700 and ILC800 is higher than the defined compressive strength of LC. From Table 4, it can be deduced that as the

dry density of concrete increases, compressive and tensile strength as well as the elastic modulus of concrete also increases. This increase in strength is due to the decrease in the amount of ECLAs and *w*/*c* ratio and increase in cement and sand content in ILC800 as compared to ILC600 and ILC700 concrete.

However, with the increase in dry density and strength of ILCs, thermal conductivity also increases. This indicates that in addition to reducing the density of concrete, higher ELCA content and *w*/*c* ratio can also contribute in improving the thermal performance of concrete as the volume of entrained air has been kept constant in each type of ILC.

Table 4: Mechanical and thermal properties of ILCs [28] and NC

Property	ILC 600	ILC 700	ILC 800	NC (C30/37)
Dry density (g/cm^3)	600	700	800	2188
Cylinder compressive strength (MPa)	5.30	9.41	12.96	30.20
Tensile strength (MPa)	0.65	0.76	0.87	2.91
Elastic modulus (MPa)	2300	3100	3900	31900
Thermal conductivity coefficient (W/mK)	0.141	0.166	0.193	1.40

3.2 Dry shrinkage strains in ILCs

Variation of drying shrinkage of every specimen for each concrete grade recorded at 2, 3, 7, 14, 28, 50, 100 days of concrete age and the average shrinkage results are presented in Figure 3. As the shrinkage strains become constant after 100 days, therefore, the shrinkage strain value at 100 days has been referred as the ultimate strain. It can be observed in Figure 3 that the average shrinkage strains in ILCs are significantly higher than that of NC, whose shrinkage strains range

between 0.2 mm/m to 0.8 mm/m. Also, shrinkage strains in ILCs terminated faster than NC because of relatively low cement content in ILCs.

As it is seen from Figure 3, the shrinkage strains in each type of ILC follow the same trend and initial shrinkage strains in each ILC are almost the same during the first 7 days. However, a clear distinction was observed between these shrinkage strains after the first week. ILC800 with higher dry density exhibited higher shrinkage strains at 100 days as compared to ILC700 and ILC600 with lower density. Although *w*/*c* ratio of ILC800 is lower than that of ILC700 and ILC600, however, the overall water and cement content are significantly higher. This higher water and cement content increases the amount of water available for evaporation and cement for shrinkage in the concrete mix. Similarly, the amount of expanded clay lightweight aggregates (ECLAs) also affects shrinkage strains. Greater the volume of ECLAs, lower is the volume reduction and consequently lower are the shrinkage strains in the ILC mix. As the content of ECLAs increases with decrease in ILC density, the shrinkage strains in ILC600 are low as compared to ILC700 which are also lower than that of ILC800.

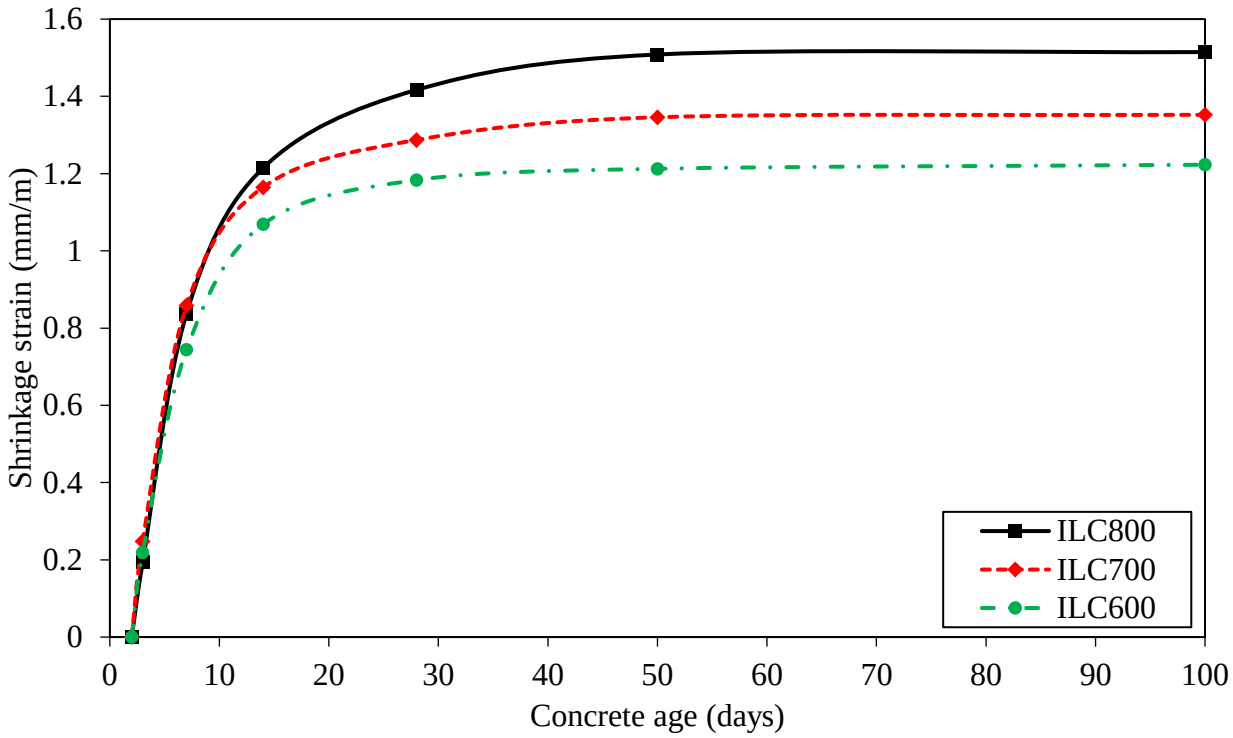

Figure 3: Experimental shrinkage strains for ILC600, ILC700 and ILC800

3.3 Dry shrinkage strains in ILC with CFRP reinforcements

Shrinkage strains of ILC600, ILC700 and ILC800 reinforced with carbon fiber reinforced polymer (CFRP) grids and their comparisons with normal ILCs are presented in Figure 4 a, b & c. For each type of CFRP grid arrangement i.e. CFRP-21 and CFRP-25, three specimens have been prepared and average results are presented. It is evident from Figure 4 that the addition of CFRP grids to ILC significantly reduces the initial shrinkage strains and strains at 100 days. However, the effect of CFRP on controlling the shrinkage of concrete depends on the cross-sectional area of FRP reinforcement in ILC. CFRP-21 grid with width and depth of 21 mm has cross-sectional area of 85 mm^2/m with corresponding reinforcement ratio of 0.45 %. Similarly, the CFRP-25 grid has cross-sectional area of 142 mm^2/m and reinforcement ratio of 0.89 %. Due to smaller cross-

sectional area per unit length and reinforcement ratio, the effect of CFRP-21 in controlling the shrinkage is also less as compared to CFRP-25.

For ILC600, shrinkage strain at 100 days reduced from 1.2 mm/m to 0.56 mm/m for CFRP-21 and 0.41 mm/m for CFRP-25 (Figure 4a). Similarly, the shrinkage strain at 100 days in ILC700 reduced to 0.71 mm/m for CFRP-21 and 0.48 mm/m for CFRP-25 from 1.35 mm/m for normal ILC700 (Figure 4b). Similar trend was observed for ILC800, where 100 days shrinkage strains reduced to 0.81 mm/m for CFRP-21 and 0.54 mm/m for CFRP-25 from 1.51 mm/m for normal ILC800 (Figure 4c). This indicates that for a reinforcement ratio of 0.45% as in case of CFRP-21, the shrinkage strains reduce by 53%, 47% and 46% for ILC600, ILC700 and ILC800 respectively. In case of CFRP-25, reinforcement ratio of 0.89 % reduces the shrinkage strains by 66%, 64% and 64% for ILC600, ILC700 and ILC800 respectively.

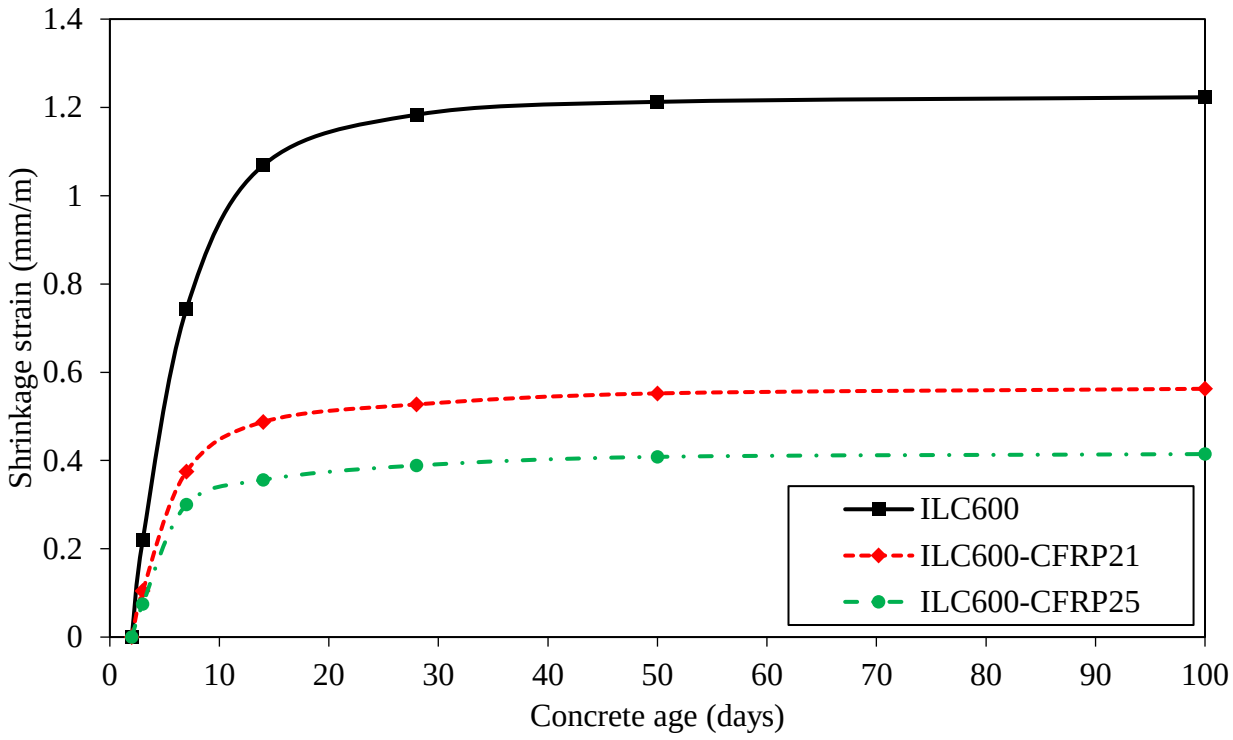
Shrinkage strain (mm/m)
Concrete age (days)
ILC600
ILC600-CFRP21
ILC600-CFRP25

(a)

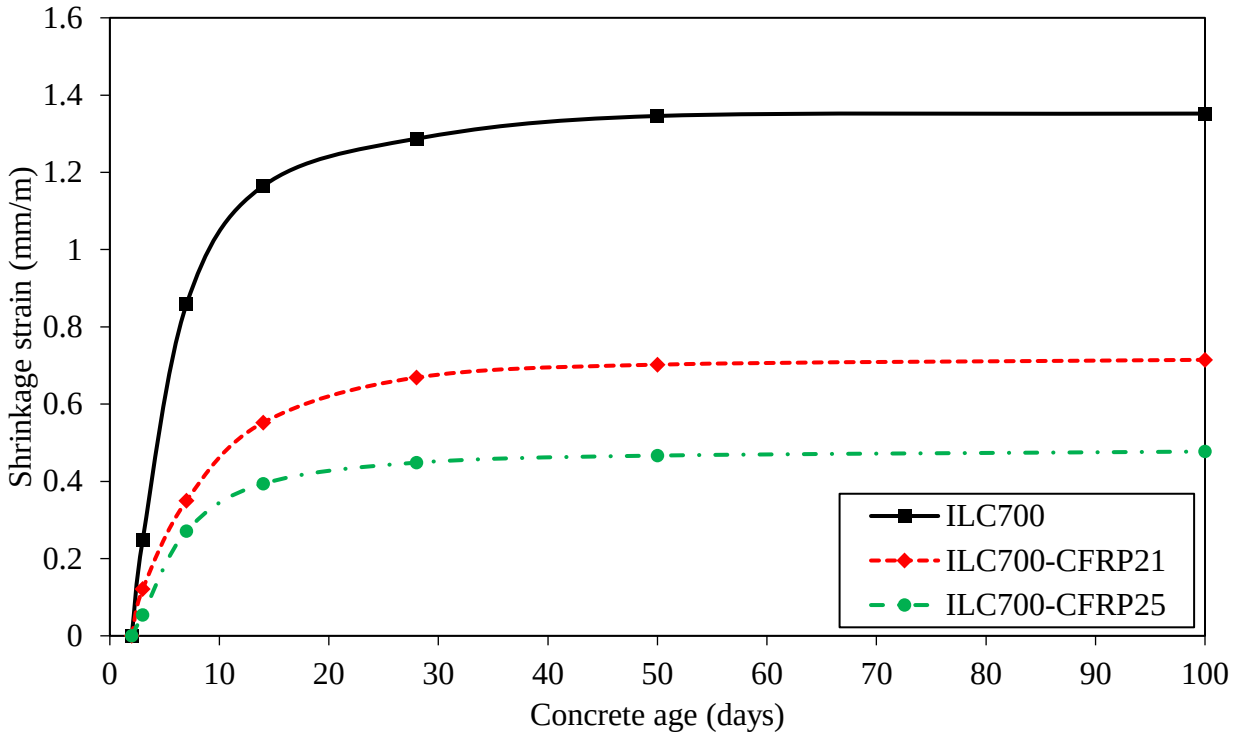
Shrinkage strain (mm/m)
Concrete age (days)
ILC700
ILC700-CFRP21
ILC700-CFRP25

(b)

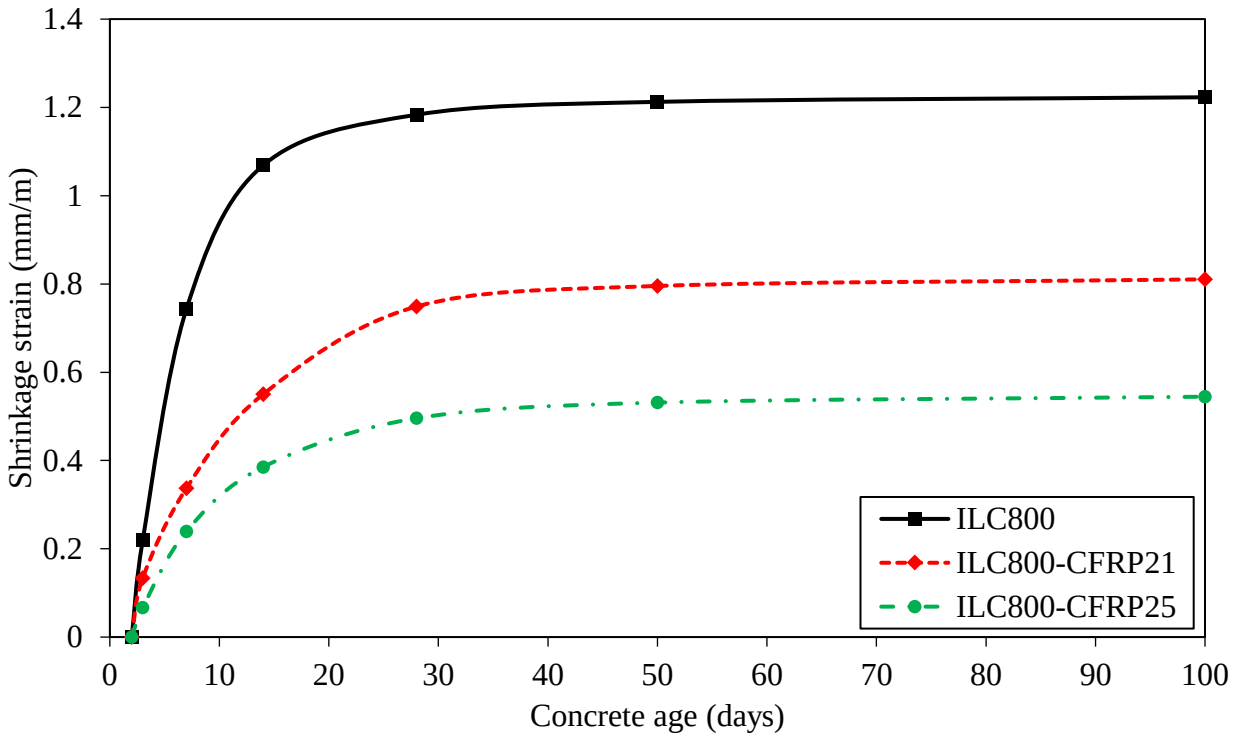

(c)

Figure 4: Experimental shrinkage strains in normal and CFRP reinforced ILCs (a) ILC600 (b) ILC700 (c) ILC800

3.4 Dry shrinkage strains in ILC with GFRP reinforcements:

The shrinkage control of ILCs with Glass fiber reinforced polymers (GFRPs) was similar to that of CFRPs, however, their efficiency in controlling the shrinkage was less than the corresponding CFRP grid reinforcement. The shrinkage strains of GFRP reinforced ILC600, ILC700 and ILC800 are presented in Figure 5. The shrinkage control efficiency of GFRP reinforcement also depends on its cross-sectional area per unit length as well as the reinforcement ratio. GRFP-21 grid with a reinforcement ratio of 0.46 % reduces the shrinkage strains by 42%, 35% and 29% for ILC600, ILC700 and ILC800 respectively. Similarly, the GFRP-25 grid with a reinforcement ratio of 0.91% reduced the shrinkage strains by 59%, 50% and 50% for ILC600, ILC700 and ILC800 respectively.

This shrinkage control efficiency of FRP grids can be attributed to axial stiffness (*EA*/*L*) provided by them. For example, the axial stiffness of GFRP-21 is the lowest which can be calculated by (60 GPa × 7.3 mm^2 / 150mm = 2.92 kN/mm). Similarly, the axial stiffness (*EA*/*L*) of CFRP-21, GFRP-25 and CFRP-25 are 5.71, 5.80 and 11.36 kN/mm respectively.

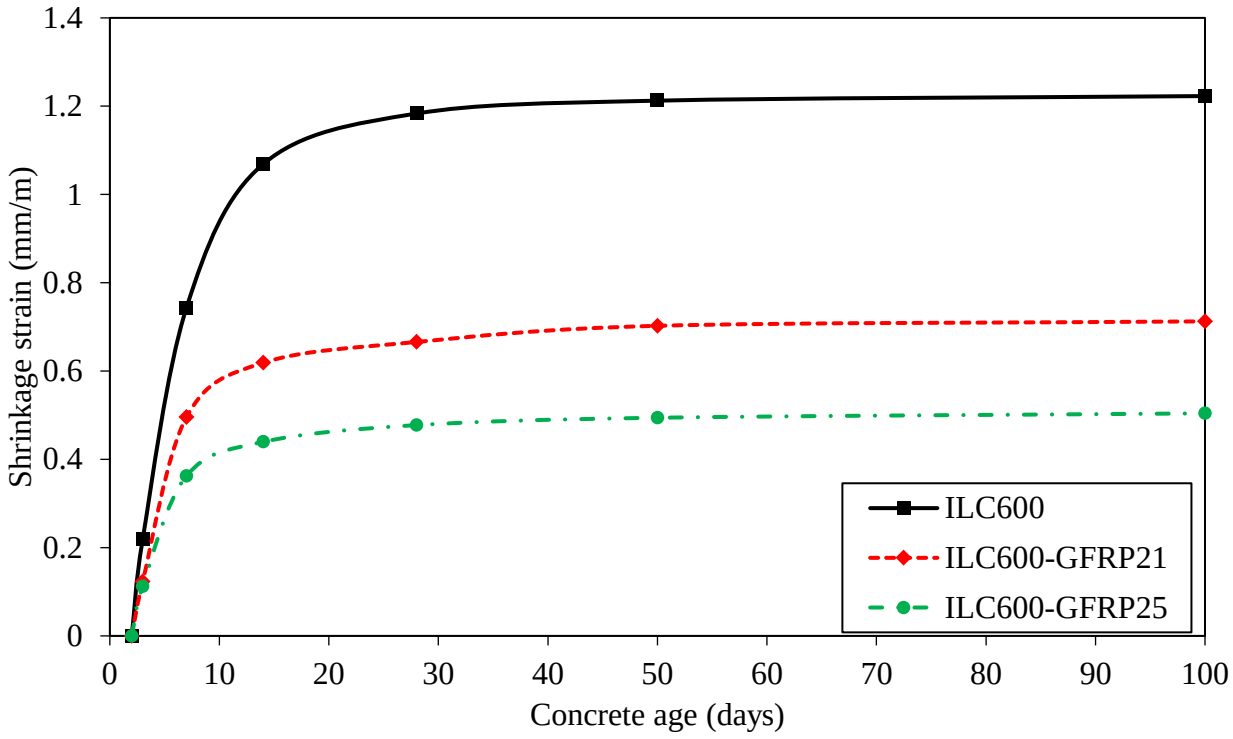

(a)

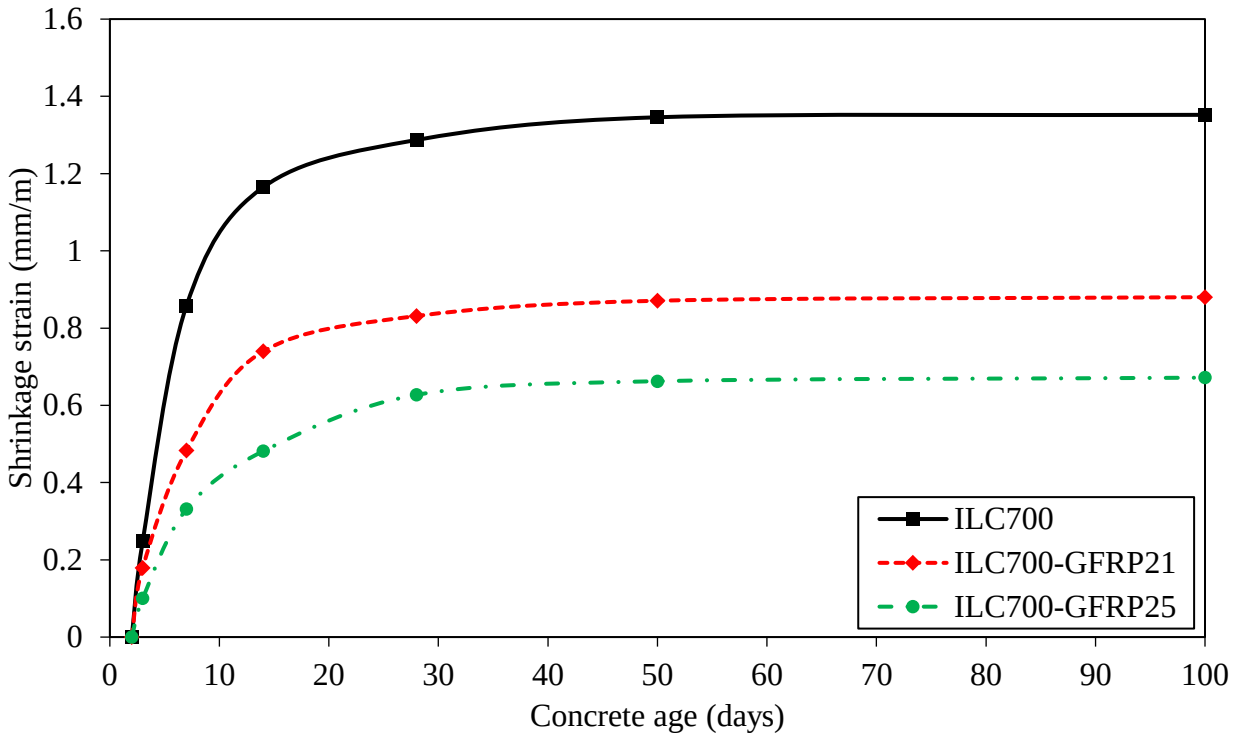
Shrinkage strain (mm/m)
Concrete age (days)
ILC700
ILC700-GFRP21
ILC700-GFRP25

(b)

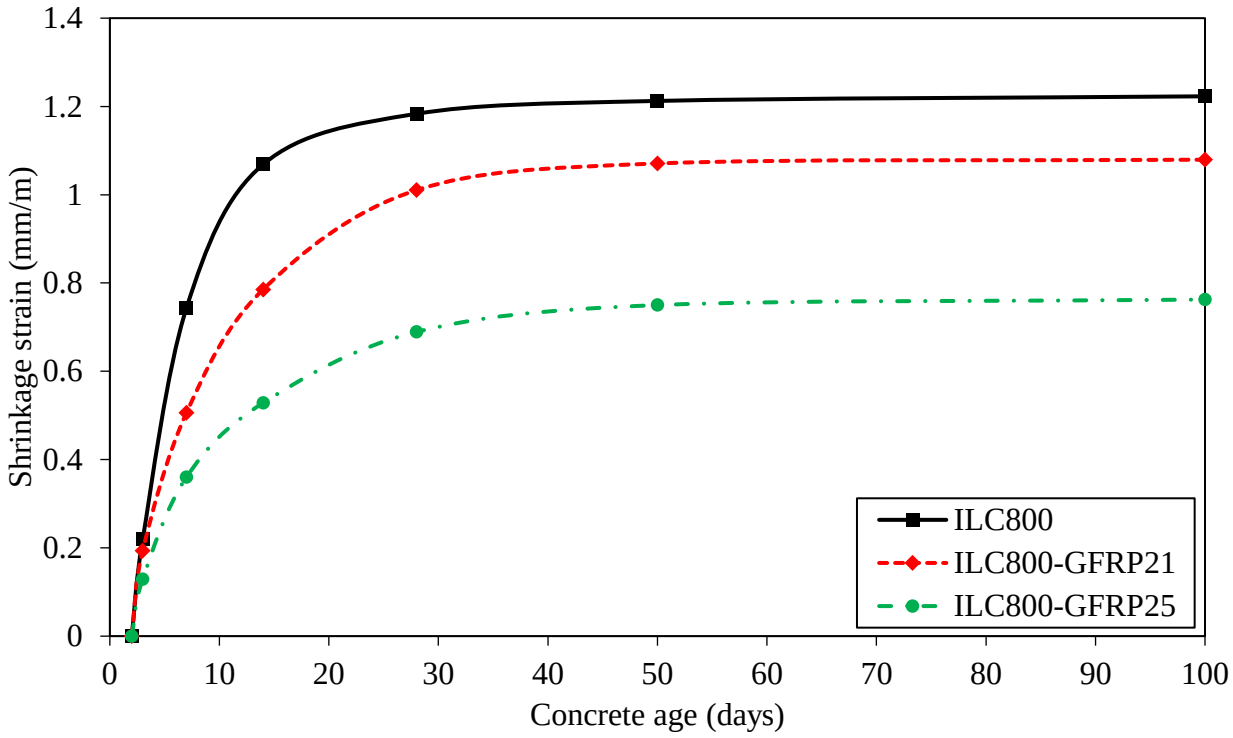
Shrinkage strain (mm/m)
Concrete age (days)
ILC800
ILC800-GFRP21
ILC800-GFRP25

(c)

Figure 5: Experimental shrinkage strains in normal and GFRP reinforced ILCs (a) ILC600 (b) ILC700 (c) ILC800

From the graphs presented in Figure 4 and Figure 5 and ultimate shrinkage strains i.e. shrinkage strain at 100 days presented in Table 5, it can be observed that reduction of shrinkage using GFRP-21 is the lowest, the shrinkage reduction values of GFRP-25 are similar to that of CFRP-21 as the axial stiffness of both these FRP grids is approximately equal, whereas the reduction of shrinkage is highest using CFRP-25 grids.

Table 5: Ultimate shrinkage strain comparison in normal and FRP reinforced ILCs and % reduction in FRP reinforced ILCs

	Normal	CFRP-21		CFRP-25		GFRP-21		GFRP-25	
	mm/m	mm/m	%	mm/m	%	mm/m	%	mm/m	%
ILC600	1.22	0.56	54.10	0.41	66.39	0.71	41.80	0.50	59.02
ILC700	1.35	0.71	47.41	0.47	65.19	0.88	34.81	0.67	50.37
ILC800	1.51	0.81	46.36	0.54	64.24	1.08	28.48	0.76	49.67

4. Prediction Models for shrinkage

Prediction of concrete shrinkage at different stages of its life is crucial for its serviceability and durability design. This shrinkage of concrete depends on a number of factors including *w*/*c* ratio, the compressive strength of concrete, curing conditions of concrete, and environmental conditions. In this part of the research program, experimentally obtained shrinkage strains have been compared with four commonly used shrinkage prediction models i.e. the ACI 209R-92 model [22], the CEB

MC90-99 model [23], the Eurocode-2 model [24] and the B3 model [25]. All of these models calculate shrinkage as a function of time and depend on a number of factors including mix design, curing conditions and environmental conditions etc. All the parameters associated with each shrinkage model were assessed during experimentation along with shrinkage strain values and the accuracy of these models has been assessed by comparing with experimentally obtained values of shrinkage.

4.1 Existing Prediction Models

4.1.1 ACI 209R-92 model:

ACI 209R-92 model [22] was initially developed for precast-prestressing industry and is recommended by ACI 209 Committee for creep and shrinkage prediction of NC and LC. It is an empirical method based on a large number of laboratory data obtained under steady humidity and loading conditions. The shrinkage calculation using this model depends on concrete composition and initial curing involving variables like type of cement, slump, percentage of fine aggregates, air content, cement content, type of curing and relative humidity. The shrinkage strain at any time (t) can be calculated by Eq. 1.

$$\varepsilon_{sh}\left(t,t_c\right)=\frac{\left(t-t_c\right)^{\alpha}}{f+\left(t-t_c\right)^{\alpha}}\varepsilon_{shu} \tag{1}$$

Where $\varepsilon_{sh}(t,t_c)$ is the shrinkage strain in mm/mm at any time, ε_{shu} is the ultimate (in time) shrinkage strain in mm/mm, t is the concrete age, t_c is the concrete curing time, α is a considered constant for a given member shape and size that define the time-ratio part, ACI 209R-92 recommends an average value of 1.0 for α. f (in days) is a considered constant for a given member shape and size that define the time-ratio part.

4.1.2 CEB MC90-99 model:

The CEB MC90-99 model [23] is recommended by the Euro-International Committee for Concrete (CEB). The model was revised in 1999 to include high-strength concretes and to separate the total shrinkage into its autogenous and drying shrinkage components. This model is applicable for shrinkage prediction of ordinary concrete having 28 days compressive strength ranging from 12 to 80 MPa under relative humidity of 40–100% and mean temperature of 5–30^{o}C. The total shrinkage at any time (t) can be calculated by using Eq. 2.

$$\varepsilon_{cs}\left(t,t_s\right)=\varepsilon_{cs0}\beta_s\left(t,t_s\right) \tag{2}$$

Where ε_{cs0} is the notional shrinkage coefficient, $\beta_s(t,t_s)$ is the coefficient to describe the development of shrinkage with time, t is the age of concrete in days and t_s is the age of concrete (days) at the beginning of shrinkage.

4.1.3 Eurocode 2 model:

The Eurocode 2 model [24] is based on the CEB MC90-99 model [23]. However, some modifications are done in the Eurocode 2 model. According to the Eurocode 2, the development of the drying shrinkage strain in time is calculated by Eq. 3.

$$\varepsilon_{cd}(t)=\beta_{ds}\left(t,t_s\right)k_h\varepsilon_{cd,0} \tag{3}$$

Where $\beta_s(t,t_s)$ is the coefficient to describe the development of shrinkage with time, t is the age of concrete (days), t_s is the age of concrete (days) at the beginning of shrinkage, k_h is a coefficient depending on the notional size and $\varepsilon_{cd,0}$ is the basic drying shrinkage. The final drying shrinkage values for LC are then obtained by multiplying the values of shrinkage strains of NC by a factor η_3 which is 1.5 for LC16/18 and 1.2 for LC 20/22.

4.1.4 B3 model:

The B3 model, as well as the B1 model and the B2 model, is the culmination of work from Bažant and his team, started in the 1970s [25]. This model complies with the general guidelines formulated by RILEM TC-107ß1. The mean shrinkage strain in time in this model is calculated by Eq. 4.

$$\varepsilon_{sh}(t,t_0) = \varepsilon_{sh\infty} k_h S(t) \tag{4}$$

Where $\varepsilon_{sh\infty}$ is the ultimate shrinkage strain, k_h is the coefficient depending on humidity and $S(t)$ is the coefficient to describe the development of shrinkage with time.

4.1.5 AS3600 model:

The Australian Standard for Concrete Structures (AS3600-2018) [26] including the revision proposed by Gilbert [42] for high strength concrete is applicable for concrete with the characteristic compressive strength in the range of 20 to 100 MPa. This model calculates the drying and autogenous shrinkage separately. The total shrinkage at any time t (in days) can be calculated by adding these two shrinkages using Eq. 5.

$$\varepsilon_{cs}(t) = \left(1 - e^{-0.07t}\right) \varepsilon^{*}_{cse} + k_1 k_4 \varepsilon_{csd.b} \tag{5}$$

Where ε^{*}_{cse} is the final autogenous shrinkage strain, $\varepsilon_{csd.b}$ is the basic drying shrinkage strain, k_1 is a coefficient associated with the time and specimen shape, k_4 is a coefficient that accounts for the environmental influence and e is the base number of natural logarithm.

4.2 Results of existing predictions models:

The drying shrinkage strains for each ILC have been calculated using all the four prediction models and compared with experimental results. This comparison of prediction models with experimental results is presented in Figure 6 a, b & c for ILC600, ILC700 and ILC800 respectively. Large

variation can be observed between the shrinkage strains predicted by models and experimentally obtained shrinkage. However, predictions of B3 models are closest to experimental values and the difference of predicted shrinkage is 25 %, 29 % and 31 % for ILC600, ILC700 and ILC800 respectively.

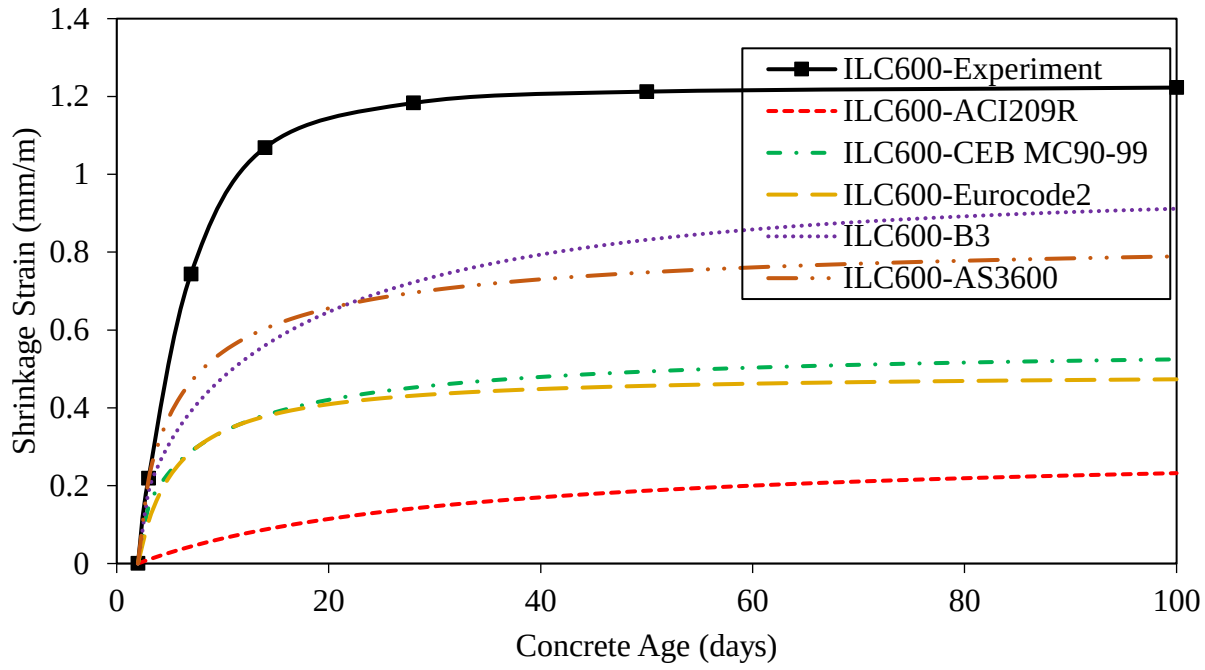

(a)

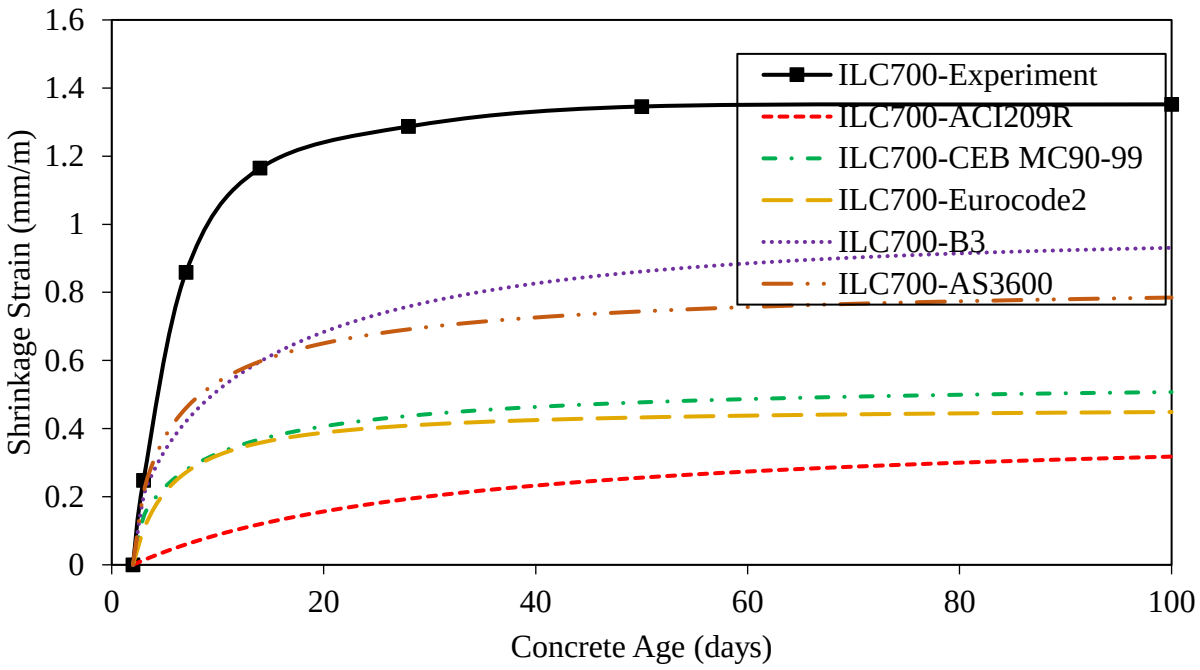
Shrinkage Strain (mm/m)
Concrete Age (days)
ILC700-Experiment
ILC700-ACI209R
ILC700-CEB MC90-99
ILC700-Eurocode2
ILC700-B3
ILC700-AS3600

(b)

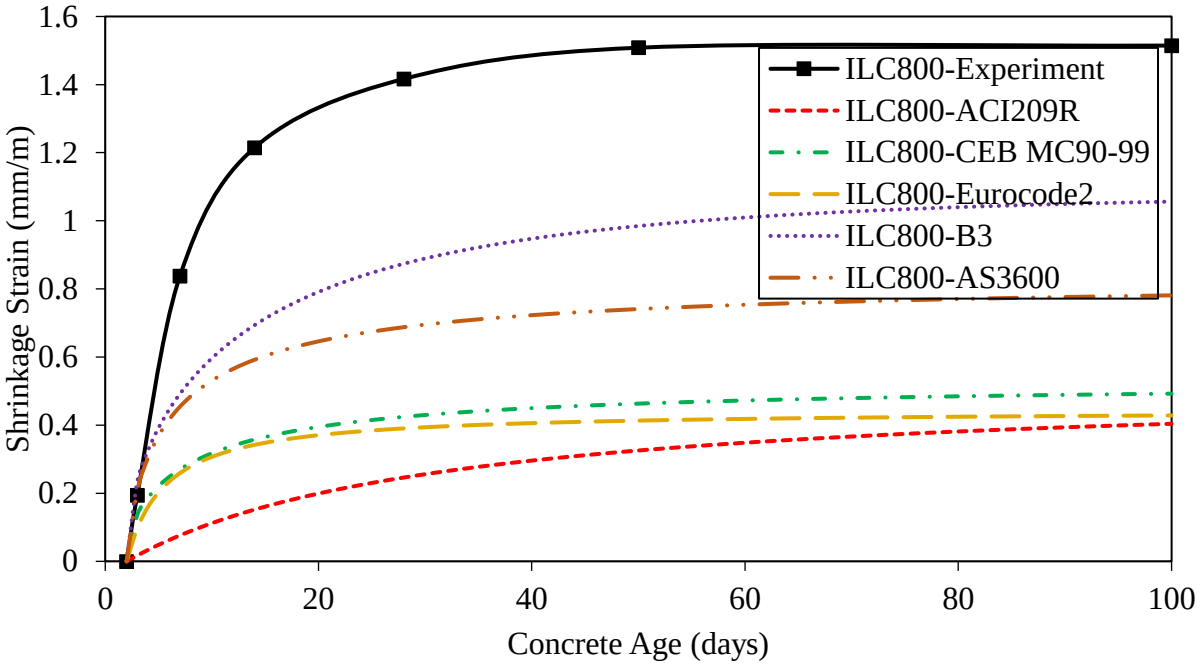
Shrinkage Strain (mm/m)
Concrete Age (days)
ILC800-Experiment
ILC800-ACI209R
ILC800-CEB MC90-99
ILC800-Eurocode2
ILC800-B3
ILC800-AS3600

(c)

Figure 6: Comparison of experimental shrinkage strains with existing prediction models (a) ILC600 (b) ILC700 (c) ILC800

4.3 Developed prediction model for ILC

Comparison of existing shrinkage prediction models with actual shrinkage of ILC600, ILC700 and ILC800 revealed that none of the prediction models can calculate the shrinkage strains accurately. As the results of the B3 model are closest to experimental shrinkage results for all ILCs, therefore, B3 model has been selected as a benchmark model where some modifications regarding concrete properties can be made so that shrinkage strains in ILCs can be predicted accurately.

The prediction model based on the B3 model has been developed so as to maintain the balance between accuracy and convenience and the minimum number of parameters have been introduced to account for ILC properties. As all the prediction models have been developed based on a scatter of experimental data and are only applicable in specific conditions, the application of the B3 model is also based on some qualifying conditions. These qualifying conditions include water to cement ratio (w/c), aggregate to cement ratio (a/c), the compressive strength of concrete (f_c) and cement content (c). The range of these qualifying conditions and corresponding values of ILC600, ILC700 and ILC800 are presented in Table 6. For Table 6, the amount of cement content has been adjusted to account for the presence of silica fumes. As per BS-EN-206 [38], the mass of silica fumes should be added in the mass of cement content when silica fumes to cement ratio (s/c) is less than 0.11 and the mass of silica fumes greater than 0.11 should be neglected. From comparison of ILC values with applicable range in Table 6, three distinct differences can be observed which are (i) water to cement ratio (w/c) of ILCs is in the upper range (ii) aggregate to cement ratio of ILCs is less than the applicable range (because a lot of lightweight aggregates are used in ILC. This is also the reason why the dry density of ILC is significantly lower than that of applicable range and NC) and

(iii) compressive strength of ILCs is significantly lower than that of applicable range and NC. Also, the dry density of ILC is also significantly lower than NC as well as LC. Therefore, in order to modify the B3 model for the prediction of accurate results for ILC, parameters related to water content, compressive strength and dry density have been modified.

Table 6: Qualifying conditions of B3 model and corresponding ILC values

	w/*c*	*a*/*c*	f_c (MPa)	*c* (kg/m^3)
Applicable Range	0.35-0.85	2.5-13.5	17-70	160-720
ILC600	1.03	1.78	5.30	208.68
ILC700	0.81	1.26	9.41	288.60
ILC800	0.69	0.95	12.96	369.63

According to the B3 model, mean shrinkage strain in concrete at any time (t) can be calculated by Eq. 4, described in section 4.1.5 and can be written in a simplified form as Eq. 5.

$$\varepsilon_{sh}(t,t_0) = \varepsilon_{shu} S(t) \tag{5}$$

where ε_{shu} is the mean ultimate shrinkage strain in the cross-section (Eq. 6) and $S(t)$ is the coefficient to describe the development of shrinkage with time (Eq. 7).

$$\varepsilon_{shu} = -\alpha_1\alpha_2\left(1.9\times10^{-2} w^{2.1} f_c^{-0.28} + 270\right)\frac{E(607)}{E\left[t_0 + 8.5t_0^{-0.08} f_c^{-0.25}(k_s D)^2\right]} k_h \times 10^{-6} \tag{6}$$

$$S(t) = \tanh\sqrt{\frac{t-t_0}{8.5t_0^{-0.08} f_c^{-0.25}(k_s D)^2}} \tag{7}$$

Where α_1 is a coefficient which takes into account cement type (1.0 for type I cement, 0.85 for type II cement and 1.1 for type III cement, where the cement type is accordance with the ASTM C150 [35], α_2 is a coefficient depending on type of curing (0.75 for steam-curing, 1.2 for sealed or normal curing in air with initial protection against drying and 1.0 for curing in water or at 100% relative humidity), w is the water content (kg/m^3), f_c is the 28-day standard cylinder compressive strength of concrete, $E(t)$ is the elastic modulus of the concrete at t day of concrete age, t_0 is the age of concrete (days) at the beginning of shrinkage, k_s is the cross-section shape factor, D is the effective cross-section thickness and k_h is the factor for humidity.

In order to consider the effect of water content (w), compressive strength (f_c) and dry density, Eq. 6 and Eq. 7 of the B3 model has been modified as Eq. 8 and Eq. 9, respectively.

$$\varepsilon_{shu} = -\alpha_1\alpha_2\left(1.9\times10^{-2}\, w^{\beta_1} f_c^{\beta_2} + 270\right)\frac{E(607)}{E\left[t_0 + 8.5t_0^{-0.08} f_c^{\beta_3}\left(k_s D\right)^2\right]} k_h \times 10^{-6} \tag{8}$$

$$S(t) = \tanh\sqrt{\frac{\rho}{\beta_4}\frac{t-t_0}{8.5t_0^{-0.08} f_c^{\beta_3}\left(k_s D\right)^2}} \tag{9}$$

In these equations, four additional parameters (β_1, β_2, β_3 and β_4) have been introduced to account for variations in water content, compressive strength and dry densities of ILC for shrinkage prediction. These parameters have been obtained through a universal global optimization algorithm (UGOA) instead of a local optimization algorithm (LOA) to prevent the influence of the initial values of parameters and obtain the global optimal solution [43]. After numerous iterations,

obtained values of these parameters were 2.125 for β_1, -0.113 for β_2, 0.633 for β_3 and 54.3 for β_4. Considering these values, shrinkage strains in ILC can be calculated by Eq. 5, Eq. 8 and Eq. 9.

Shrinkage strains of ILC600, IL700 and ILC800 of this research program were calculated using Eqs. 5, 8 and 9 and these predictions were compared with experimental results and are presented in Figure 7. It can be seen that the modified model can predict the values quite accurately with a difference of 2%, 3% and 4% for ILC 600, ILC 700 and ILC 800 respectively. Also, the predicted shrinkage strain at 100 days was slightly higher than experimental shrinkage strains which implies that predictions of modified B3 are also safe.

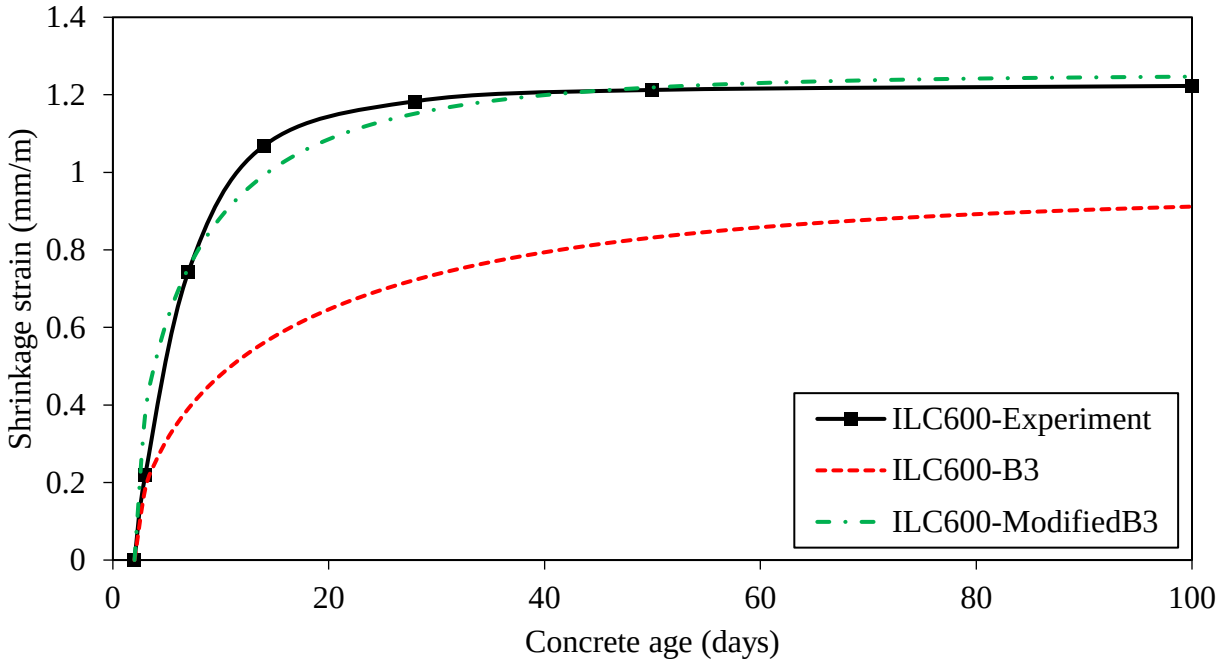

(a)

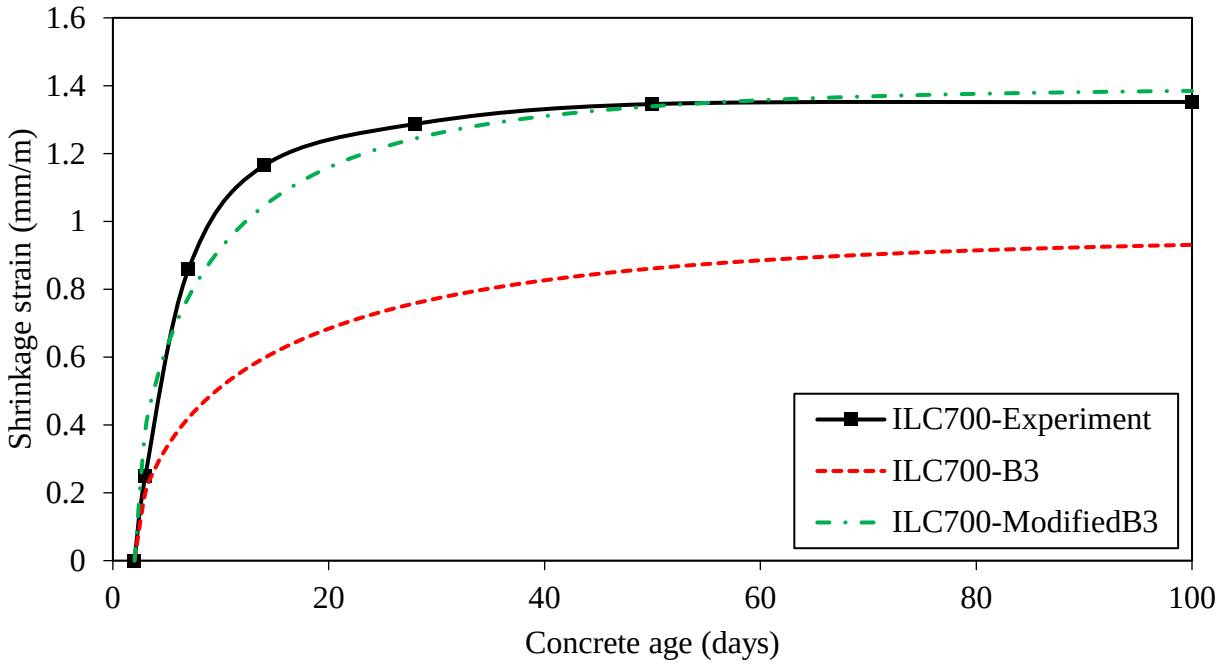
Shrinkage strain (mm/m)
Concrete age (days)
ILC700-Experiment
ILC700-B3
ILC700-ModifiedB3

(b)

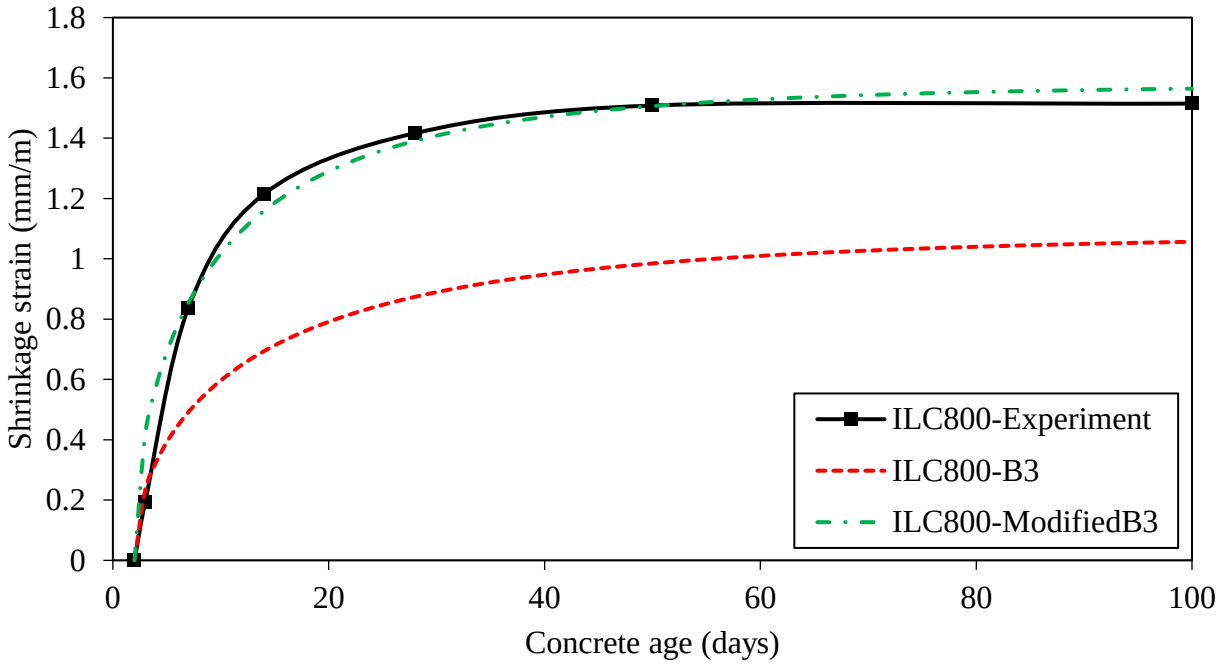
Shrinkage strain (mm/m)
Concrete age (days)
ILC800-Experiment
ILC800-B3
ILC800-ModifiedB3

(c)

Figure 7 Comparison of modified prediction model with B3 model and experimental results (a) ILC600 (b) ILC700 (c) ILC800

4.3 Developed prediction model for FRP grids reinforced ILC

To control the shrinkage strain in ILC, ILCs have been reinforced with FRP reinforcement grids and a significant reduction in shrinkage strains has been observed. Prediction of shrinkage strains of ILCs reinforced with FRP grids is also crucial to ascertain the serviceability and durability of structures. The existing prediction models don't take into account the presence of reinforcement and thus can only be applied to NC. In this research program, the prediction model for ILCs reinforced with FRP grids has also been developed for convenient and accurate prediction of shrinkage and compared with experimental results.

From the experimental results of shrinkage strains for four types of FRP reinforcements i.e. CFRP-21, CFRP-25, GFRP-21 and GFRP-25, it has been found that CFRP-25 is most efficient in controlling the shrinkage strains and reduction of shrinkage strains depend on the axial stiffness of FRP grid. Therefore, the shrinkage prediction model of FRP reinforced ILC has been developed by including the stiffness proportion of reinforcement and concrete (E_rA_r/E_cA_c). Similar to normal ILC, the B3 model has been modified to predict the shrinkage strains of FRP reinforced ILC. The shrinkage strains in FRP reinforced ILCs can be calculated by using Eq. 10.

$$\varepsilon_{sh}'(t,t_0) = k_r \varepsilon_{sh}(t,t_0) \tag{10}$$

where $\varepsilon_{sh}'(t,t_0)$ is the shrinkage value strain in FRP reinforced ILC, $\varepsilon_{sh}(t,t_0)$ is the shrinkage strain in only ILC obtained through experimental tests or using Eq. 5 and k_r is a coefficient that takes into account the influence of the reinforcement on the shrinkage value of ILC and can be calculated by using Eq. 11.

$$k_r = r^{\varphi} \tag{11}$$

where r is the ratio of cross-sectional stiffness of reinforcement and cross-sectional stiffness of concrete (E_rA_r/E_cA_c) and φ is the coefficient obtained by regression analysis of experimental data. Based on this regression analysis, a linear relationship was derived between φ and r (Figure 8) presented by Eq. 12.

$$\varphi = 3.298r\text{-}0.133 \tag{12}$$

Based on the linear Eq. 12, Eq. 11 can then be written as Eq. 13.

$$k_r = r^{3.298r\text{-}0.133} \tag{13}$$

Shrinkage strains reinforced ILCs can then be calculated by using Eq. 10 and Eq. 13. Experimentally measured shrinkage strains of FRP reinforced ILC600, ILC700 and ILC 800 are presented in Figure 9, Figure 10 and Figure 11 respectively. The comparison of shrinkage strains with the modified prediction model shows that the modified model can calculate the shrinkage strains quite accurately and can be adopted of shrinkage prediction of ILC reinforced with any type of reinforcement.

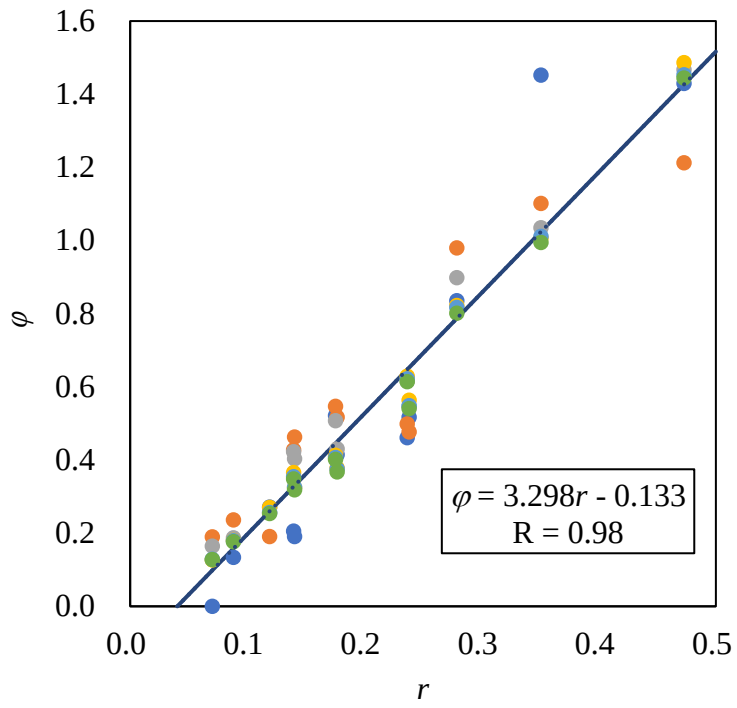

Figure 8: Multivariate linear regression of r and φ

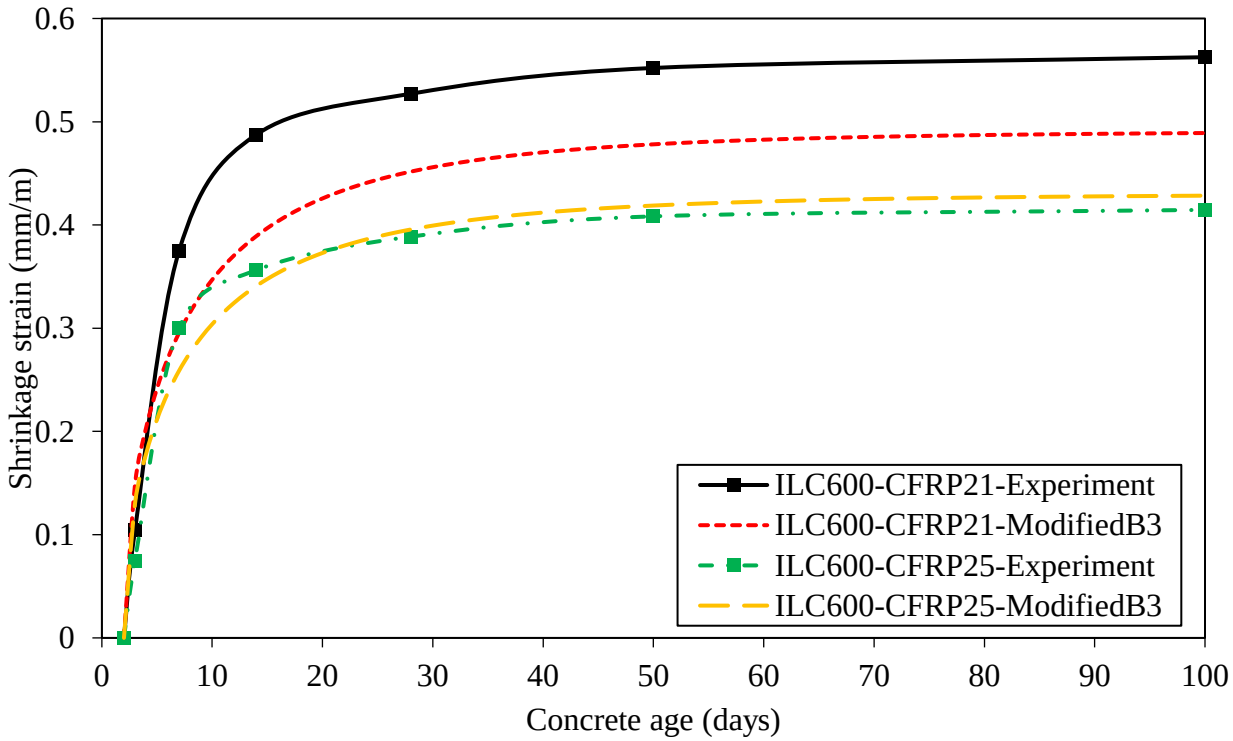

(a)

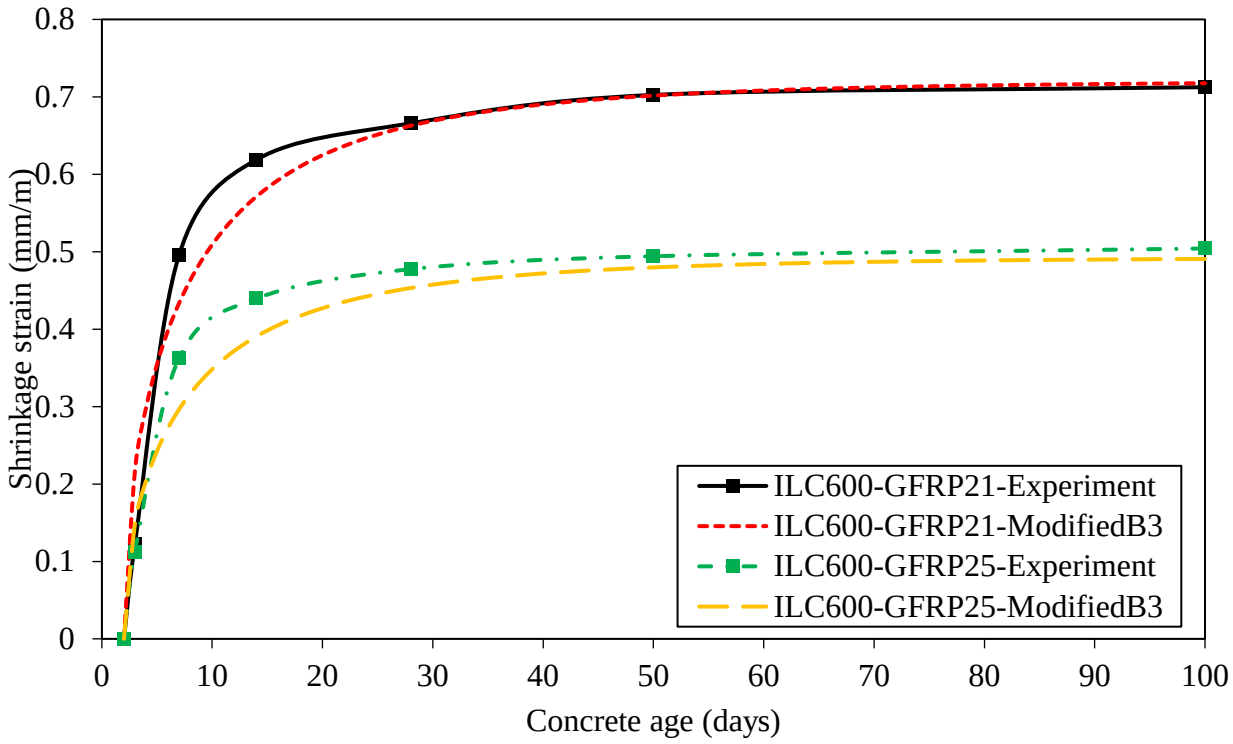

(b)

Figure 9: Comparison of modified prediction model for FRP reinforced ILC600 with experimental results (a) ILC600-CFRP and (b) ILC600-GFRP

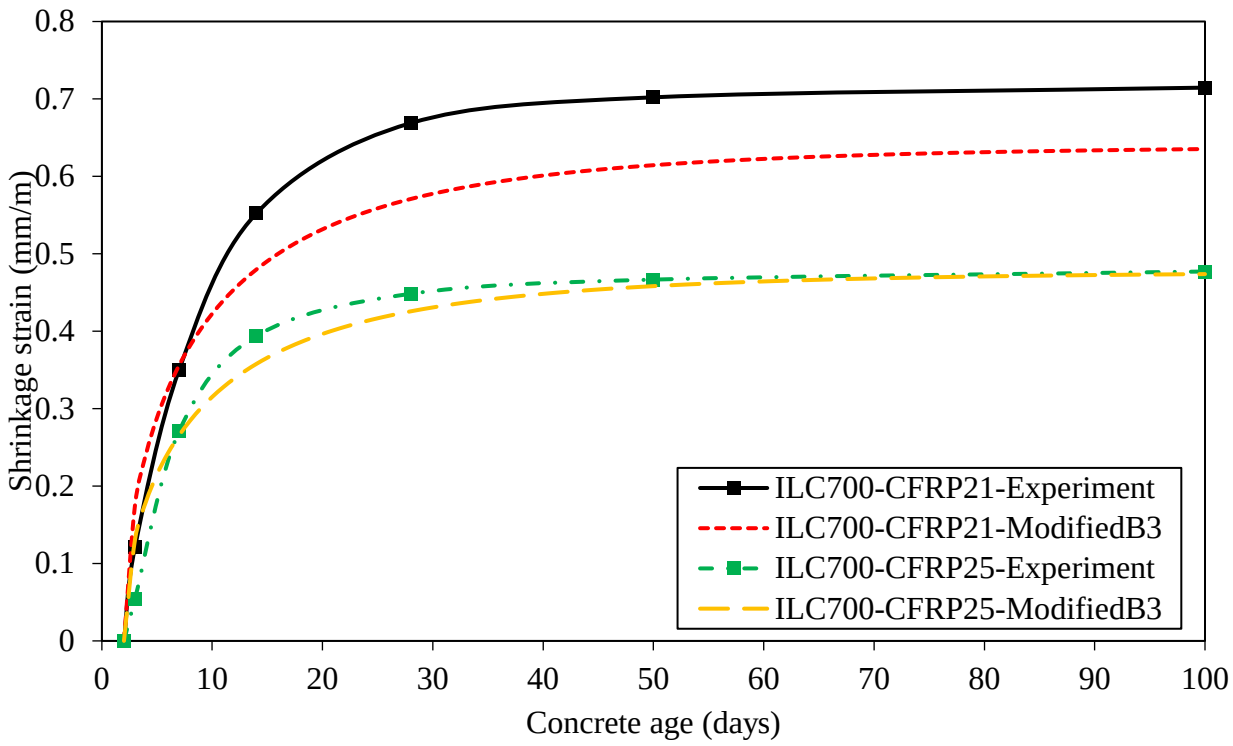
0.8
0.7
0.6
0.5
0.4
0.3
0.2
0.1
0
Shrinkage strain (mm/m)
0
10
20
30
40
50
60
70
80
90
100
Concrete age (days)
ILC700-CFRP21-Experiment
ILC700-CFRP21-ModifiedB3
ILC700-CFRP25-Experiment
ILC700-CFRP25-ModifiedB3

(a)

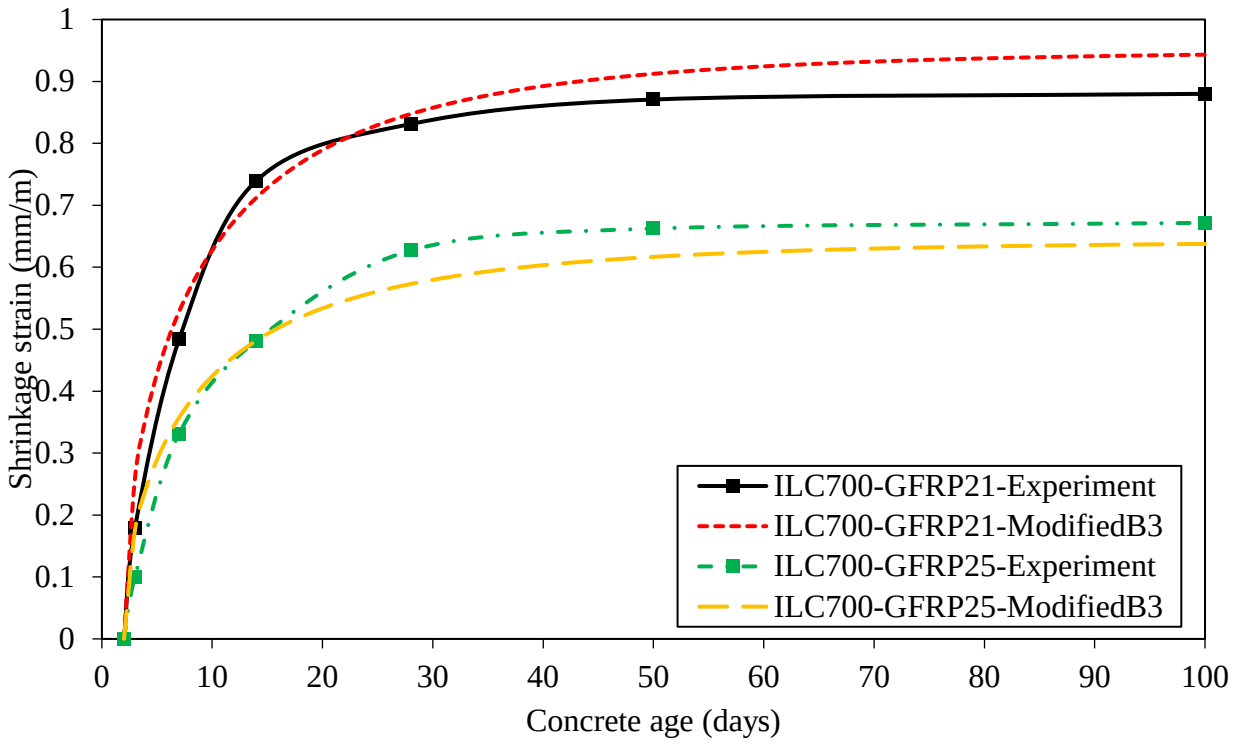

(b)

Figure 10: Comparison of modified prediction model for FRP reinforced ILC700 with experimental results (a) ILC700-CFRP and (b) ILC700-GFRP

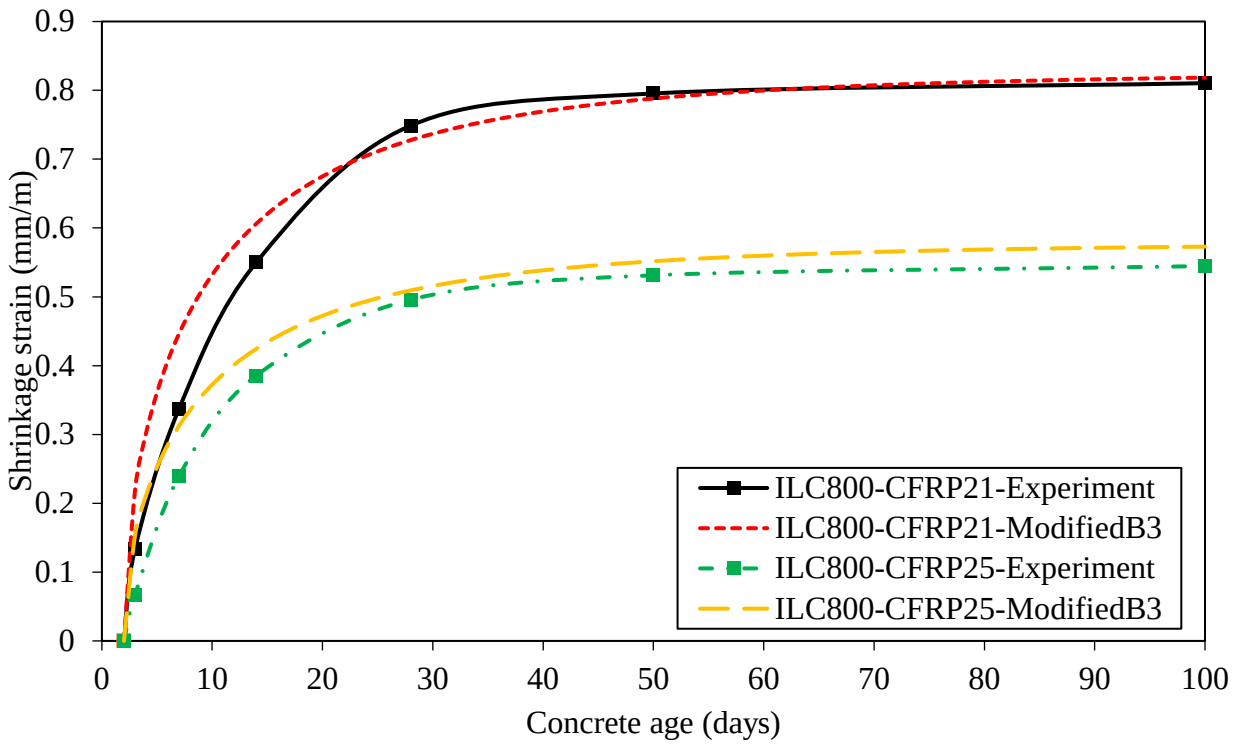
0.9
0.8
0.7
0.6
0.5
0.4
0.3
0.2
0.1
0
Shrinkage strain (mm/m)
0
10
20
30
40
50
60
70
80
90
100
Concrete age (days)
ILC800-CFRP21-Experiment
ILC800-CFRP21-ModifiedB3
ILC800-CFRP25-Experiment
ILC800-CFRP25-ModifiedB3

(a)

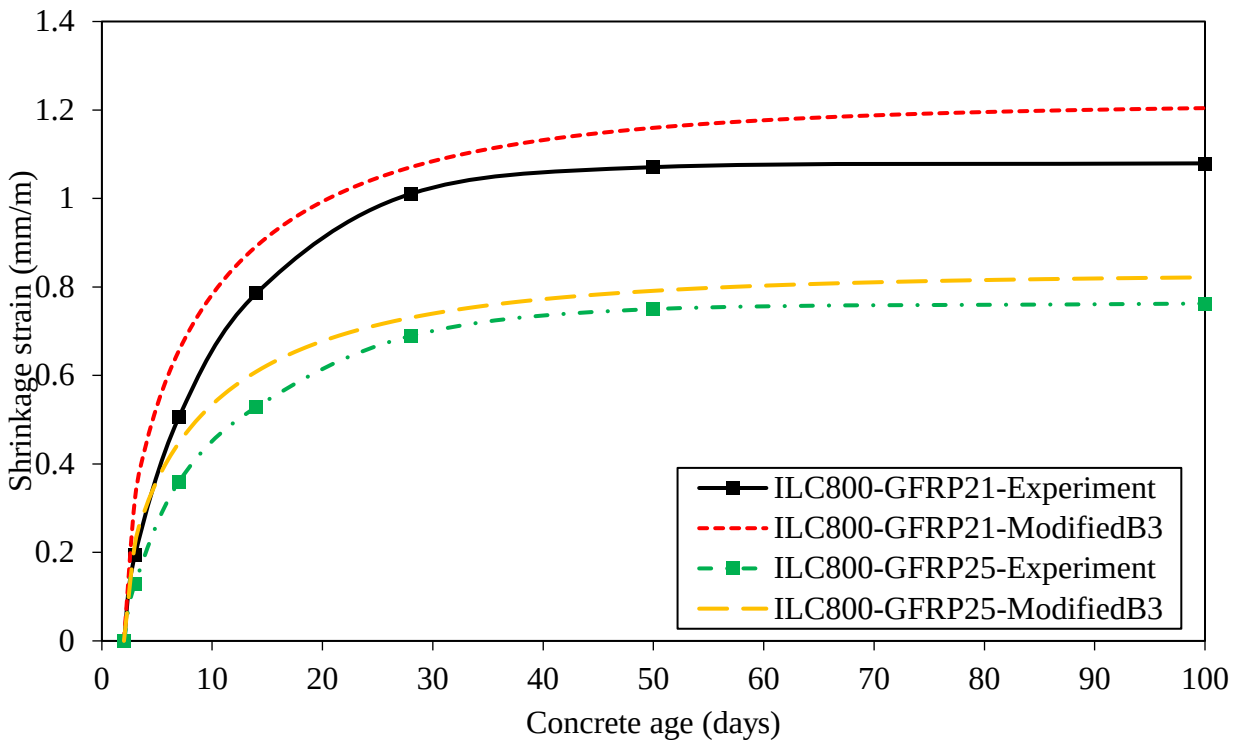

(b)

Figure 11: Comparison of modified prediction model for FRP reinforced ILC800 with experimental results (a) ILC800-CFRP and (b) ILC800-GFRP

5. Conclusions:

Three types of ILCs have been manufactured as an alternative to NC for efficient structural solutions and named as ILC600, ILC700 and ILC800. The low weight of ILCs is obtained by a relatively higher *w*/*c* ratio and replacing normal aggregates with expanded lightweight clay aggregates (ELCAs). These ILCs have been then reinforced with two types of FRPs i.e. CFRP and GFRP and two different grid arrangements have been used for each type of FRP namely CFRP-21, CFRP-25, GFRP-21 and GFRP-25. Experimental and theoretical studies conducted on these ILCs lead to the following conclusions:

- Due to relatively high water to cement ratios of ILCs as compared to NC, drying shrinkage strains are also high and measured ultimate strains i.e. strains at the age of 100 days for ILC600, ILC700 and ILC800 are 1.23, 1.35 and 1.51 mm/m respectively. These shrinkage strains are significantly higher than the strains in NC which range from 0.2 to 0.8 mm/m. Although the *w*/*c* ratio in ILC800 is lowest amongst the three ILCs, shrinkage strains are highest because of the higher content of cement and water. Also, ELCAs are lowest in ILC800 which also results in its higher shrinkage and higher dry density.
- Although all FRP grid reinforcements are effective as they reduced the shrinkage strains significantly and close to the shrinkage strains of NC, CFRP-25 grid reinforcement is most effective as it reduced the shrinkage strains up-to the maximum level and close to shrinkage strains of NC.
- The effect of FRP grid reinforcement on shrinkage reduction depends on axial stiffness (*EA*/*L*) of FRP grid reinforcement. The axial stiffness of CFRP-21, CFRP-25, GFRP-21 and GFRP-25 are 5.71, 11.36, 2.92 and 5.80 kN/mm respectively. The lowest axial stiffness of GFRP-21 has resulted in its least impact on shrinkage reduction of ILC. However, the highest axial stiffness of CFRP-25 has resulted in maximum shrinkage reduction of CFRP-25 reinforced ILC.
- Comparison of experimental shrinkage strains with four presently available prediction models has exhibited that none of the prediction models can calculate the shrinkage strains accurately. However, predictions of the B3 model are closest to experimental values and the same model has been modified to take into account the water content, compressive strength and dry density of ILC. Four new factors have been introduced in the modified model and comparison of the modified model with experimental shrinkage strains has

proved its accuracy for ILC. Therefore, the modified model can be utilized for any type of ILC.

- Another prediction model has been developed based on the modified B3 model to take into account the effect of FRP reinforcement. This prediction model uses a correction factor k_r based on the cross-sectional stiffness of FRP reinforced concrete (E_rA_r/E_cA_c). Accuracy of the modified prediction model for FRP reinforced concrete has been assessed by comparing its results with experimental results. The modified prediction model is found to be accurate and can be utilized for ILCs reinforced with any type of reinforcement.

As the prediction models have been developed based on limited test data, therefore, future experimental studies are recommended where experimental shrinkage in both the normal and reinforced ILCs can be compared with developed prediction models.

Acknowledgement:
The authors gratefully acknowledge the financial support provided by the Bundesministerium für Bildung und Forschung, German project (03ZZ0305O) and the National Natural Science Fundation of China Youth Science Foundation Project (NSFC 51908012).

References:

[1] C. Meyer, "The greening of the concrete industry," *Cem. Concr. Compos.*, vol. 31, no. 8, pp. 601–605, 2009, doi: 10.1016/j.cemconcomp.2008.12.010.

[2] W. H. Kwan, M. Ramli, K. J. Kam, and M. Z. Sulieman, "Influence of the amount of recycled coarse aggregate in concrete design and durability properties," *Constr. Build. Mater.*, vol. 26, no. 1, pp. 565–573, 2012, doi: 10.1016/j.conbuildmat.2011.06.059.

[3] V. Kodur and W. Khaliq, "Effect of temperature on thermal properties of different types of

high-strength concrete," *J. Mater. Civ. Eng.*, vol. 23, no. 6, pp. 793–801, 2011, doi: 10.1061/(ASCE)MT.1943-5533.0000225.

[4] J. Newman and P. Owens, "Properties of lightweight concrete," in *Advanced Concrete Technology*, 2003, pp. 72–99.

[5] Y. W. Choi, Y. J. Kim, H. C. Shin, and H. Y. Moon, "An experimental research on the fluidity and mechanical properties of high-strength lightweight self-compacting concrete," *Cem. Concr. Res.*, vol. 36, no. 9, pp. 1595–1602, 2006, doi: 10.1016/j.cemconres.2004.11.003.

[6] S. Caijun and W. Yanzhong, "Mixture oportioning and Properties of Self-Consolidating Lightweight Concrete Containing Glass Powder," *ACI Mater. J.*, vol. 102, no. 5, p. 355, 2005.

[7] O. M. Jensen, "Influence of cement composition on autogenous deformation and change of the relative humidity," in *Proc. Shrinkage 2000—Int. RILEM Workshop on Shrinkage of Concrete*, 2000, pp. 143–153.

[8] A. M. Neville, *Properties of concrete*, 5th ed. Pearson, 2010.

[9] H. Reinhardt and J. Kümmel, "Some tests on creep and shrinkage of recycled lightweight aggregate concrete," vol. 10, pp. 9–22, 1999.

[10] T. C. Hansen and E. Boegh, "Elasticity and Drying Shrinkage Concrete of Recycled-Aggregate," *J. Proc.*, vol. 82, no. 5, pp. 648–652, 1985.

[11] O. Kayali, M. N. Haque, and B. Zhu, "Drying shrinkage of fibre-reinforced lightweight aggregate concrete containing fly ash," *Cem. Concr. Res.*, vol. 29, no. 11, pp. 1835–1840,

1999, doi: 10.1016/S0008-8846(99)00179-9.

[12] S. P. Shh, M. E. Krguller, and M. Sarigaphuti, “Effects of Shrinkage-Reducing Admixtures on Restrained Shrinkage Cracking of Concrete,” *Mater. J.*, vol. 89, no. 3, pp. 289–295, 1992.

[13] M. Shoya, S. Sugita, and T. Sugawara, “Improvement of drying shrinkage and shrinkage cracking of concrete by special surfactants.,” in *Proceedings of the international symposium held by RILEM (The International Union of Testing and Research Laboratories for Materials and Structures)*, 1990, pp. 484–495.

[14] N. S. Berke, M. P. Dallaire, M. C. Hicks, and A. Kerkar, “New Deveopments in Shrinkage-Reducing Admixtures,” *Spec. Publ.*, vol. 173, pp. 973–1000, 1997.

[15] T. Tafsirojjaman, S. Fawzia, D. Thambiratnam, and X. L. Zhao, “Seismic strengthening of rigid steel frame with CFRP,” *Arch. Civ. Mech. Eng.*, vol. 19, no. 2, pp. 334–347, 2019, doi: 10.1016/j.acme.2018.08.007.

[16] Tafsirojjaman, S. Fawzia, and D. Thambiratnam, “Enhancement Of Seismic Performance Of Steel Frame Through CFRP Strengthening,” *Procedia Manuf.*, vol. 30, pp. 239–246, 2019, doi: 10.1016/j.promfg.2019.02.035.

[17] T. Tafsirojjaman, S. Fawzia, D. Thambiratnam, and X. Zhao, “Numerical investigation of CFRP strengthened RHS members under cyclic loading,” *Structures*, vol. 24, pp. 610–626, 2020, doi: 10.1016/j.istruc.2020.01.041.

[18] T. Tafsirojjaman, S. Fawzia, D. Thambiratnam, and X. L. Zhao, “Behaviour of CFRP strengthened CHS members under monotonic and cyclic loading,” *Compos. Struct.*, vol.

220, no. February, pp. 592–601, 2019, doi: 10.1016/j.compstruct.2019.04.029.

[19] N. Banthia, “Durability enhancements in concrete with fiber reinforcement,” in *Int. Conf: Sustainable construction materials and technologie*, 2007, pp. 209–219.

[20] L. Dvorkin and O. Dvorkin, *Basics of Concrete Science*. St. Petersburg (Russia), 2006.

[21] X. F. Wang, C. Fang, W. Q. Kuang, D. W. Li, N. X. Han, and F. Xing, “Experimental investigation on the compressive strength and shrinkage of concrete with pre-wetted lightweight aggregates,” *Constr. Build. Mater.*, vol. 155, pp. 867–879, 2017, doi: 10.1016/j.conbuildmat.2017.07.224.

[22] A. C. Institute, *Guide for Modeling and Calculating Shrinkage and Creep*. American Concrete Institute, 2008.

[23] C. E. D. B. International, *CEB-FIP Model Code 1990*. 1993.

[24] *Eurocode 2 – Design of concrete structures*. 2004.

[25] Z. P. Bazant and W. P. Murphy, “Creep and shrinkage prediction model for analysis and design of concrete structures - model B3,” *Mater. Constr.*, vol. 28, no. 180, pp. 357–365, 1995, doi: 10.1007/bf02486204.

[26] S. Australia, “AS 3600-2018: Concrete Structures.” Standards Australia Limited Sydney, NSW, 2018.

[27] R. V. Silva, J. De Brito, and R. K. Dhir, “Prediction of the shrinkage behavior of recycled aggregate concrete: A review,” *Constr. Build. Mater.*, vol. 77, pp. 327–339, 2015, doi: 10.1016/j.conbuildmat.2014.12.102.

[28] A. Hückler and M. Schlaich, “Structural Behavior of Reinforced Infra-Lightweight

Concrete (ILC)," *ACI Struct. J.*, vol. 116, no. 2, pp. 3–14, 2019.

[29] M. Schlaich and M. E. Zareef, "Infraleichtbeton," *Beton- und Stahlbetonbau*, vol. 103, no. 3, pp. 175–182, 2008, doi: 10.1002/best.200700605.

[30] M. Schlaich and A. Hückler, "Infraleichtbeton 2.0," *Beton- und Stahlbetonbau*, vol. 107, no. 11, pp. 757–766, 2012, doi: 10.1002/best.201200033.

[31] C. Lösch and P. Rieseberg, *Infraleichtbeton: Entwurf, Konstruktion, Bau*. Fraunhofer IRB Press, 2018.

[32] M. Schlaich and A. Hückler, "Infraleichtbeton: Reif für die Praxis," *Beton ‐ und Stahlbetonbau*, vol. 112, no. 12, pp. 772–783, 2017.

[33] C. P. Pantelides, R. Surapaneni, and L. D. Reaveley, "Structural performance of hybrid GFRP/steel concrete sandwich panels," *J. Compos. Constr.*, vol. 12, no. 5, pp. 570–576, 2008, doi: 10.1061/(ASCE)1090-0268(2008)12:5(570).

[34] Y. Shao and A. Mirmiran, "Control of plastic shrinkage cracking of concrete with carbon fiber-reinforced polymer grids," *J. Mater. Civ. Eng.*, vol. 19, no. 5, pp. 441–444, 2007, doi: 10.1061/(ASCE)0899-1561(2007)19:5(441).

[35] ASTM, "ASTM C150: Standard specification for Portland cement," 2001.

[36] A. C. I. Committee, "Building code requirements for structural concrete (ACI 318-08) and commentary," 2008.

[37] British Standards Institution, *BS EN 12390-7:2000 Part 7: Density of hardened concrete*, vol. 3, no. 1. 2000.

[38] European Committee for Standardization (CEN), *BS EN 206-1:2000 Concrete - Part 1: Specification, performance and conformity*, vol. 3. 2000.

[39] B. S. E. N. 196-1: 2016, "Methods of testing cement. Part 1: Determination of strength." BSI Standards Limited, 2016.

[40] B. S. E. N, "12390-13. Testing hardened concrete–Part 13: determination of secant modulus of elasticity in compression," *Br. Stand. Inst. London, UK*, 2013.

[41] BS EN 12617–4:2002, "Products and systems for the protection and repair of concrete structures. Test methods, Determination of Shrinkage and Expansion," *Br. Stand. Inst.*, pp. 1–18, 2002.

[42] R. I. Gilbert, "Creep and Shrinkage Models for High Strength Concrete – Proposals for Inclusion in AS3600," *Aust. J. Struct. Eng.*, vol. 4, no. 2, pp. 95–106, 2002, doi: 10.1080/13287982.2002.11464911.

[43] H. Tuy and N. T. Hoai-Phuong, "Optimization under composite monotonic constraints and constrained optimization over the effecient set," in *Global Optimization: From Theory to Implementation*, L. Liberti and L. Maculan, Eds. Springer, pp. 5–31.